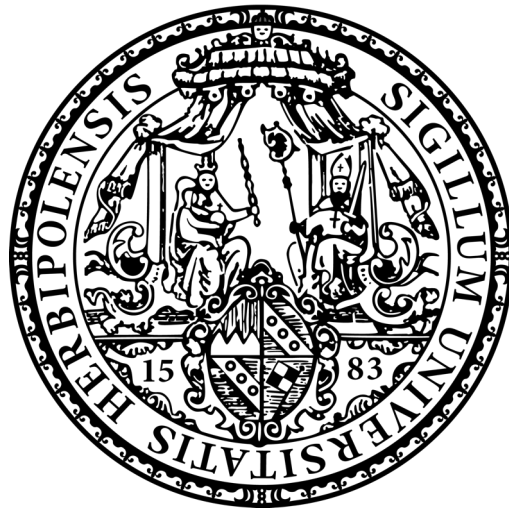


Characterization of a novel putative factor involved in
host adaptation in *Trypanosoma brucei*

by
Zdenka Cicova



A dissertation submitted in partial fulfillment
of the requirements for the degree of
Doctor of Philosophy
(Biology)
at the Julius Maximilian University of Wuerzburg
2016

Doctoral Committee:

Prof. Christian Janzen

Prof. Klaus Brehm

Characterization of a novel putative factor involved in
host adaptation in *Trypanosoma brucei*

Dissertation zur Erlangung des
naturwissenschaftlichen Doktorgrades
der Julius-Maximilians-Universität Würzburg

vorgelegt von

Zdenka Cicova

Aus Jablonec nad Nisou (Tschechische Republik)

Würzburg, 2016

Eingereicht am: 25. Juli 2016

Mitglieder der Promotionskommission:

Vorsitzender: Prof. Dr. Thomas Rudel,
Dekan der Fakultät für Biologie

Gutachter: Prof. Christian Janzen

Gutachter: Prof. Klaus Brehm

Tag des Promotionskolloquiums: 7. Dezember 2016

Doktorurkunde ausgehändigt am:

Cicova, Zdenka
Bozener Straße 6
815 47 München
Tel. 017662393801
E-Mail: zdenka.cicova@centrum.cz

Erklärungen nach §4 Abs. 3 Satz 3, 5, 8 der Promotionsordnung der Fakultät für Biologie

Affidavit

I hereby declare that my thesis entitled: "**Characterization of a novel putative factor involved in host adaptation in *Trypanosoma brucei***" is the result of my own work.

I did not receive any help or support from commercial consultants. All sources and / or materials applied are listed and specified in the thesis.

Furthermore I verify that the thesis has not been submitted as part of another examination process neither in identical nor in similar form.

Eidesstattliche Erklärung

Hiermit erkläre ich an Eides statt, die Dissertation: „**Characterization of a novel putative factor involved in host adaptation in *Trypanosoma brucei***“, eigenständig, d. h. insbesondere selbständig und ohne Hilfe eines kommerziellen Promotionsberaters, angefertigt und keine anderen, als die von mir angegebenen Quellen und Hilfsmittel verwendet zu haben.

Ich erkläre außerdem, dass die Dissertation weder in gleicher noch in ähnlicher Form bereits in einem anderen Prüfungsverfahren vorgelegen hat.

Würzburg, den 24.5.2016

Unterschrift

1 Statement of authenticity

I, Zdenka Cicova, declare that the work: Characterization of a novel putative host adaptation factor in *Trypanosoma brucei*, submitted here is my own and expressed in my own words except where declared otherwise. I did not receive any help or support from commercial consultants. Any work used by any other author(s) in any form has been properly acknowledged where used. A list of all the references used has also been included. This work has not already been submitted for any degree and is not being submitted concurrently for any degree.

Collaborators in this project:

Falk Butter (Quantitative Proteomics, Institute of Molecular Biology (IMB), Mainz, Germany)

Tomas Skalicky (Laboratory of Molecular Biology of Protists, Institute of Parasitology Biology Centre, ASCR, Ceske Budejovice, Czech Republic)

Name: Zdenka Cicova

Signature:

Place and date: Würzburg 24.5.2016

2 Abstract

Trypanosomes are masters of adaptation to different host environments during their complex life cycle. Large-scale proteomic approaches provide information on changes at the cellular level in a systematic way. However, a detailed work on single components is necessary to understand the adaptation mechanisms on a molecular level. Here we have performed a detailed characterization of a bloodstream form (BSF) stage-specific putative flagellar host adaptation factor (Tb927.11.2400) identified previously in a SILAC-based comparative proteome study. Tb927.11.2400 shares 38% amino acid identity with *TbFlabarin* (Tb927.11.2410), a procyclic form (PCF) stage specific flagellar BAR domain protein. We named Tb927.11.2400 *TbFlabarin* like (*TbFlabarinL*) and demonstrate that it is a result of a gene duplication event, which occurred in African trypanosomes. *TbFlabarinL* is not essential for growth of the parasites under cell culture conditions and it is dispensable for developmental differentiation from BSF to the PCF *in vitro*. We generated a *TbFlabarinL*-specific antibody and showed that it localizes in the flagellum. The co-immunoprecipitation experiment together with a biochemical cell fractionation indicated a dual association of *TbFlabarinL* with the flagellar membrane and the components of the paraflagellar rod.

3 Zusammenfassung

Trypanosomen zeigen sich im Laufe ihres komplexen Lebeszyklus als Meister der Adaption an verschiedene Umweltbedingungen ihrer Wirte. Umfangreiche proteomische Analysen geben systematisch Auskunft über Änderungen auf zellulärer Ebene. Detaillierte Arbeit an einzelnen Komponenten ist jedoch nötig, um die Adaptionsmechanismen auf molekularer Ebene zu verstehen. Wir haben im Rahmen dieser Arbeit eine detaillierte Charakterisierung eines stadienspezifischen mutmaßlich flagellaren Wirtsadptionsfaktors der Blutstromform (BSF) durchgeführt (Tb927.11.2400), der zuvor in einer SILAC-basierten vergleichenden Proteomstudie identifiziert wurde. Tb927.11.2400 teilt 38% der mit *TbFlabarin* (Tb927.11.2410), eines stadienspezifischen flagellaren BAR-domänen Proteins der prozyklischen Form (PCF). Wir haben Tb927.11.2400 *TbFlabarin* like (*TbFlabarinL*) genannt und zeigen, dass es das Ergebnis eines Genduplikations-Ereignisses darstellt, das in afrikanischen Trypanosomen aufgetreten ist. *TbFlabarinL* ist nicht essentiell für das Wachstum der Parasiten unter Zellkultur-Bedingungen und entbehrlich für den Differenzierungsprozess von BSF zu PCF *in vitro*. Wir haben einen *TbFlabarinL*-spezifischen Antikörper entwickelt und zeigen, dass er in der Flagelle lokalisiert. Das Co-immunoprecipitations-Experiment deutet zusammen mit einer biochemischen Zellfraktionierung darauf hin, dass *TbFlabarinL* mit der flagellaren Membran und Komponenten der paraflagellaren Stab binär assoziiert ist.

4 Acknowledgements

In the first place I would like to thank Christian Janzen for giving me the opportunity and trust to join his lab in Würzburg. It brought me all the way to this point and I am very grateful for it. It was exciting to work on such an interesting and challenging project. I learned a whole lot along the way. I appreciate not only the scientific guidance but also the support in the difficult life situations.

I thank

...Falk Butter, Mario Dejung, Tomas Skalicky and Brooke Morriswood for the collaboration on this project

...Markus Engstler, Susanne Kramer, Tim Krüger, Nicolai Siegel, Ines Subota, Nicola Jones and Manfred Alsheimer for the scientific input

...Elisabeth Meyer Natus for technical support

...Gülcin Dindar and Andreas Anger for giving me the courage to take the crucial decision

...Helena Reis and Nicole Eisenhuth for being great labmates and friends

... Marius Glogger for the good times

... the whole department of cell and developmental biology

Last but not least my thanks belong to my family and friends for being there for me.

5 Table of contents

1	Statement of authenticity.....	i
2	Abstract.....	ii
3	Zusammenfassung.....	iii
4	Acknowledgements.....	iv
5	Table of contents.....	v
6	Abbreviations.....	vii
1	Introduction.....	1
1.1	Kinetoplastida and disease.....	1
1.2	<i>Trypanosoma brucei</i> cell architecture.....	2
1.3	The developmental cycle of <i>Trypanosoma brucei</i>	4
1.4	<i>Trypanosoma brucei</i> as a model organism.....	6
1.5	Host adaptation.....	7
1.6	Flagellum of <i>Trypanosoma brucei</i>	8
1.7	Aims of this thesis.....	10
2	Materials and methods.....	12
2.1	Computational analyses.....	12
2.2	Molecular cloning.....	12
2.2.1	DNA fragments amplification.....	12
2.2.2	Fragmentation of DNA molecules by restriction endonucleases.....	12
2.2.3	Separation and isolation of DNA fragments.....	13
2.2.4	Ligation of DNA fragments.....	13
2.2.5	Transformation of chemically competent <i>Escherichia coli</i>	13
2.2.6	Growth of <i>E. coli</i>	14
2.2.7	Isolation of plasmid DNA from <i>E. coli</i>	14
2.2.8	Purification of DNA.....	14
2.2.9	Purification of <i>T. brucei</i> genomic DNA.....	14
2.3	Sodium dodecyl sulfate polyacrylamide gel electrophoresis (SDS-PAGE).....	15
2.4	Western blot.....	15
2.5	Cultivation and transfection of trypanosomes.....	16
2.6	Differentiation of trypanosomes.....	17
2.7	Generation of transgenic trypanosome cell lines (Tab. 2.5).....	18
2.8	Polyclonal Antibody Generation.....	19

2.9	Immunofluorescence (IF)	20
2.10	Co-immunoprecipitation.....	21
2.11	Mass Spectrometry	21
2.12	Statistical analysis	21
2.13	Isolation of cytoskeletons and flagella	22
2.14	Chemicals.....	22
3	Results	30
3.1	<i>TbFlabarinL</i> originated from a gene duplication event.....	30
3.2	<i>TbFlabarinL</i> is not an essential gene.....	35
3.3	<i>TbFlabarinL</i> is dispensable for developmental differentiation.....	39
3.4	<i>TbFlabarinL</i> is associated with the paraflagellar rod and the flagellar membrane	43
4	Discussion.....	50
5	References.....	53

6 Abbreviations

AA	amino acid
ACP	adenylate cyclase procyclic stage specific
ADP	adenosine diphosphate
AK	arginine kinase
ApoL	apolipoprotein L
Arf	ADP ribosylation factor
BAR	Bin-Amphiphysin-Rvs
BLAST	basic local alignment search tool
<i>BLE</i>	Phleomycin resistance gene
BSF	bloodstream form
bp	base pairs
Caf	calflagin
CDS	coding sequence
COBALT	constraint-based multiple alignment tool
DNA	deoxyribonucleic acid
ER	endoplasmic reticulum
ES	expression site
EV/EVs	extracellular vesicle/extracellular vesicles
FAZ	flagellar attachment zone
FcaBP	flagellar calcium binding protein
FP	flagellar pocket
FPLC	fast protein liquid chromatography
GDP	guanosine diphosphate
GPI-PLC	glycophosphatidylinositol phospholipase
GRESAG	receptor type adenylyate cyclase
gRNA	guide RNA
HAT	human viifrican trypanosomiasis
<i>HYG</i>	hygromycin phosphotransferase gene
IMD	IRSp53 and MIM (missing in metastases) homology domain
LB	Luria Bertani
Ld	<i>Leishmania donovani</i>
LS	long slender
MC	metacaspase
MCM	Monte Carlo Markov
mRNA	messenger RNA
NCBI	National center for biotechnology information
OD	optical density
ORF	open reading frame
P	pellet
<i>PAC</i>	puromycin N-acetyl-transferase gene
PBS	phosphate buffer saline
PCF/PCFs	procyclic form/procyclics
PCR	polymerase chain reaction
PFR	paraflagellar rod

Phyre2	protein homology/analogy recognition engine
PTU/PTUs	polycistronic transcription unit/units
RNA	ribonucleic acid
RNAi	RNA interference
RT	room temperature
S	supernatant
SDS-PAGE	sodium dodecyl sulfate polyacrylamide gel electrophoresis
SIF	stumpy induction factor
SILAC	stable isotope labeling of amino acids in cell culture
SM	Single Marker
SN	supernatant
SOC	super optimal broth with catabolite repression
SRA/SRAs	serum resistance associated protein/proteins
SS	short stumpy
TAE	Tris-acetate-EDTA
Tb	<i>Trypanosoma brucei</i>
Tc	<i>Trypanosoma cruzi</i>
TDB	trypanosome dilution buffer
Tet	tetracyclin
TLF	trypanosome lytic factor
UTR	untranslated region
UV	ultraviolet
VSG	variant surface glycoprotein
WB	western blot
WT	wild type

1 Introduction

1.1 Kinetoplastida and disease

Kinetoplastida is a class of unicellular protozoa that share a common feature called kinetoplast, which consists of the mitochondrial DNA of the cell (reviewed in¹). The class Kinetoplastida includes the order of exclusively parasitic Trypanosomatida, which are either monoxenous, restricted to one host individual or dixenous and undergoing a complex life cycle between a host and a vector. Some species of this order are causative agents of various infectious diseases. They are spread in many parts of the world with a devastating impact on human health and economies of impoverished countries. For example *Leishmania spp* causes leishmaniasis in the regions of South America, South Europe, Africa and West Asia. *Trypanosoma cruzi* causes Chagas disease in South America. *Trypanosoma brucei* (*T. brucei*) is responsible for sleeping sickness in humans (HAT) or Nagana in livestock, in Sub-Saharan Africa². All three parasites are transmitted to mammals by bloodsucking insects, however they differ in the mode of infection and disease.

In contrast to *T. brucei*, *Leishmania* is an intracellular parasite transmitted by the bite of an infected female sandfly of the *Phlebotomus spp*. The parasite immediately invades several types of cells in the dermis such as macrophages, dendritic cells, neutrophils and fibroblasts (reviewed in³). There are three main forms of the disease a cutaneous, a mucocutaneous and a visceral form. The cutaneous form results in open lesions, ulcers and severe scarring of the exposed body parts. The mucocutaneous form manifests as a partial or total mutilation of mucous membranes of the nose, mouth and throat. The visceral form leads to enlargement of internal organs such as spleen and liver and in addition it affects the bone marrow leading to pancytopenia. It is lethal within two years if left untreated⁴.

Trypanosoma cruzi is another intracellular kinetoplastid parasite. It is transmitted by a contact with the feces of an infected kissing bug of the *Triatominae spp*, mostly, while the bug feeds on the blood of a human. Chagas disease manifests in two stages, an acute initial phase and a chronic phase. In the acute phase (2 months post infection) the disease shows typical symptoms such as skin lesion, swelling of the eyelids or other general unspecific symptoms (fever, muscle pain, parlor etc.) in only 50% of the cases, although large numbers of the parasite are circulating in the blood. In

the chronic phase the parasite resides within the heart muscle leading to cardiac disorder and heart failure or within the muscles of the digestive tract resulting in the enlargement of the esophagus and colon⁵.

T. brucei lives extracellularly in the blood and body fluids of vertebrates. It is transmitted by a bite of an infected tsetse fly of the *Glossina spp*, which takes a blood meal. Trypanosomes are injected into the dermis and local inflammatory reaction occurs rarely. It is known as chancre. From the dermis trypanosomes enter the bloodstream and draining lymphatics in the haemo-lymphatic stage, which involves bouts of fever, headache and itching. Trypanosomes can traverse capillaries into the connective tissue and cross the blood brain barrier into the central nervous system and cerebrospinal fluid in the meningo-encephalic stage of the disease manifested by changes of behavior, confusion, poor coordination and sleep-wake cycle disturbance⁶. In contrast to *T. brucei rhodensiense* and *T. brucei gambiense*, *T. brucei brucei* infects only game and cattle and is not infective to humans since it lacks serum resistance associated protein (SRA)⁷. SRA expression circumvents the activity of trypanosome lytic factor (TLF)⁸ of the human innate immunity. SRA neutralizes the activity of TLF by binding to apolipoprotein L-1 (ApoL-1), which is a pore forming toxin within TLF⁹. Both *T.b. rhodensiense* and *T. b. gambiense* cause HAT, however they differ in the geographical distribution and disease progression. *T.b. gambiense* is found in the West and Central Africa and causes asymptomatic chronic infection for months or years until detected in the terminal stage. It causes 98% of the cases of HAT with humans as a main reservoir of the parasite. *T.b. rhodensiense* is found within eastern and southern African countries and causes an acute form of HAT with a fast development and invasion of the central nervous system up to months after infection. *T. b. rhodensiense* has an animal reservoir and thus difficult to control. 65 million people are at risk of HAT¹⁰ however, recently the cases of HAT have declined rapidly by the control over human infections as well as efforts to eliminate the vector^{10,11}.

1.2 *Trypanosoma brucei* cell architecture

T. brucei is of a spindle shape with a single flagellum attached along the cell body (Fig. 1.1). The name trypanosoma comes from the Greek word trypano, which means auger and soma, which means body. This name was chosen because of the corkscrew like movement of the parasite mediated by the beat of the flagellum. *T. brucei* possesses many morphological features of a typical eukaryotic cell such as nucleus, nucleolus, Golgi apparatus,

endoplasmic reticulum and mitochondrion. In addition, it has special features such as glycosomes, kinetoplast, a flagellar pocket and a microtubule skeleton underlying the membrane covered by variant surface glycoprotein (VSG) coat in the bloodstream form (BSF) of the parasite. Glycosomes are diversified peroxisomes, in which the glycolytic pathway of trypanosomes takes place (reviewed in¹²). The kinetoplast is a compact disc of mitochondrial DNA composed of maxi- and minicircles. Maxicircles encode mitochondrial proteins whereas minicircles encode guide RNAs (gRNA). To become functional, the mitochondrial transcripts undergo modification by insertion or deletion of uridines in RNA editing process, where gRNAs serve as templates¹³.

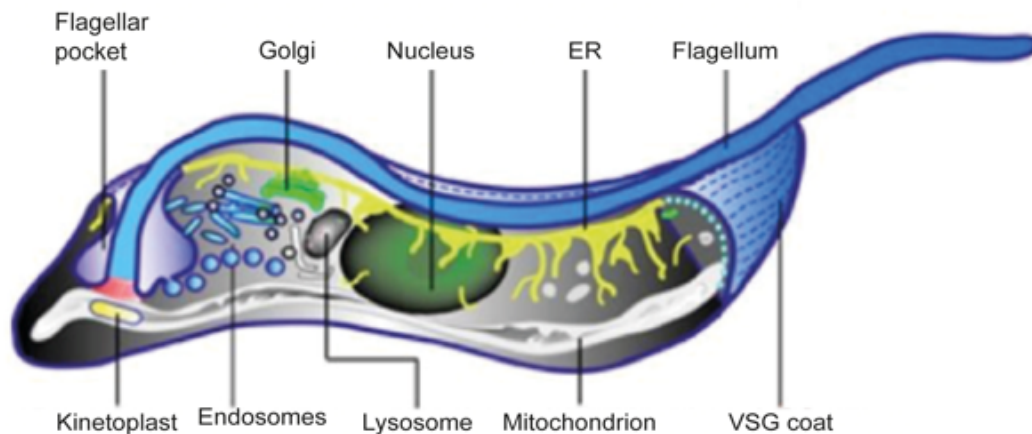


Figure 1.1. Cellular architecture of *Trypanosoma brucei* bloodstream form (adapted from Overath and Engstler 2004)

The surface of *T. brucei* is covered by a variant surface glycoprotein (VSG) coat. A microtubule corset that is found underneath the cell membrane gives the cell the spindle like shape. The cell membrane creates an invagination at the posterior end of the cell creating a flagellar pocket. The flagellum emerges from the flagellar pocket and is attached to the cell. The basal body of the flagellum is connected to the kinetoplast of the mitochondrion. ER: endoplasmic reticulum.

The kinetoplast is tethered to the basal body of the flagellum by filamentous structures¹⁴. The flagellum emerges from the flagellar pocket, which is an invagination of the cellular membrane and the exclusive site of exo- and endocytosis¹⁵. It plays an important role in the internalization and recycling of VSGs¹⁶ and in the host immune system evasion¹⁷. Most of the organelles are present in a single copy and thus *T. brucei* is a suitable model organism to study for example organelle duplication and segregation during the cell division cycle.

1.3 The developmental cycle of *Trypanosoma brucei*

In the following paragraphs the developmental cycle of *T. brucei* will be briefly overviewed together with the main aspects of morphological and metabolic features of the respective stages.

T. brucei proliferates in the blood of infected mammals as a long slender (LS) BSF. A densely packed VSG coat covers the surface of the BSF parasites. There are about 1000 VSG genes and pseudogenes present in the genome of trypanosomes¹⁸. VSG is transcribed from one of the 20 specialized subtelomeric loci called expression site (ES)¹⁹. Only one expression site is active at a time, which allows monoallelic expression of VSG²⁰. VSG is central to antigenic variation²¹ when the transcription of one VSG is switched to another. This happens by two main mechanisms, either by homologous recombination of the VSG in the active ES or by *in situ* switch when another ES is activated and the previously active one is silenced^{22,23}. Periodical changing of the VSG coat contributes together with a pronounced endocytosis and other mechanisms to the host immune system evasion^{24,25} and successful proliferation of the parasite. The parasite uses glucose present in the host body fluids as a source of energy, which is obtained via glycolysis. This takes place in a specialized peroxisome like organelle called glycosome²⁶. The mitochondrion of LS is suppressed, lacks cristae and the oxidative cytochrome chain phosphorylation is not active²⁷.

LS parasites differentiate upon a quorum sensing signal called stumpy induction factor (SIF)²⁸, via an intermediate form into a cell cycle arrested short stumpy (SS) form. The mitochondrion of SS increases in volume and tubular cristae are formed in preparation for the switch to the amino acid based metabolism in the fly²⁹. SS can be taken up by the tsetse fly and only then can they continue differentiation. In the endoperitrophic space of the fly midgut, SS form loses the VSG coat, and the cell surface is covered by procyclin³⁰. The endocytic activity ceases and the mitochondrion branches. Its volume increases from 5 to 25% of the cell³¹. The discoid cristae are formed and the cytochrome mediated oxidative chain phosphorylation becomes activated. Now proline present in the fly midgut is used as a main source of energy as opposed to glucose.

The procyclic form (PCF) trypanosomes divide rapidly and invade the ectoperitrophic space, which becomes densely packed with trypanosomes.

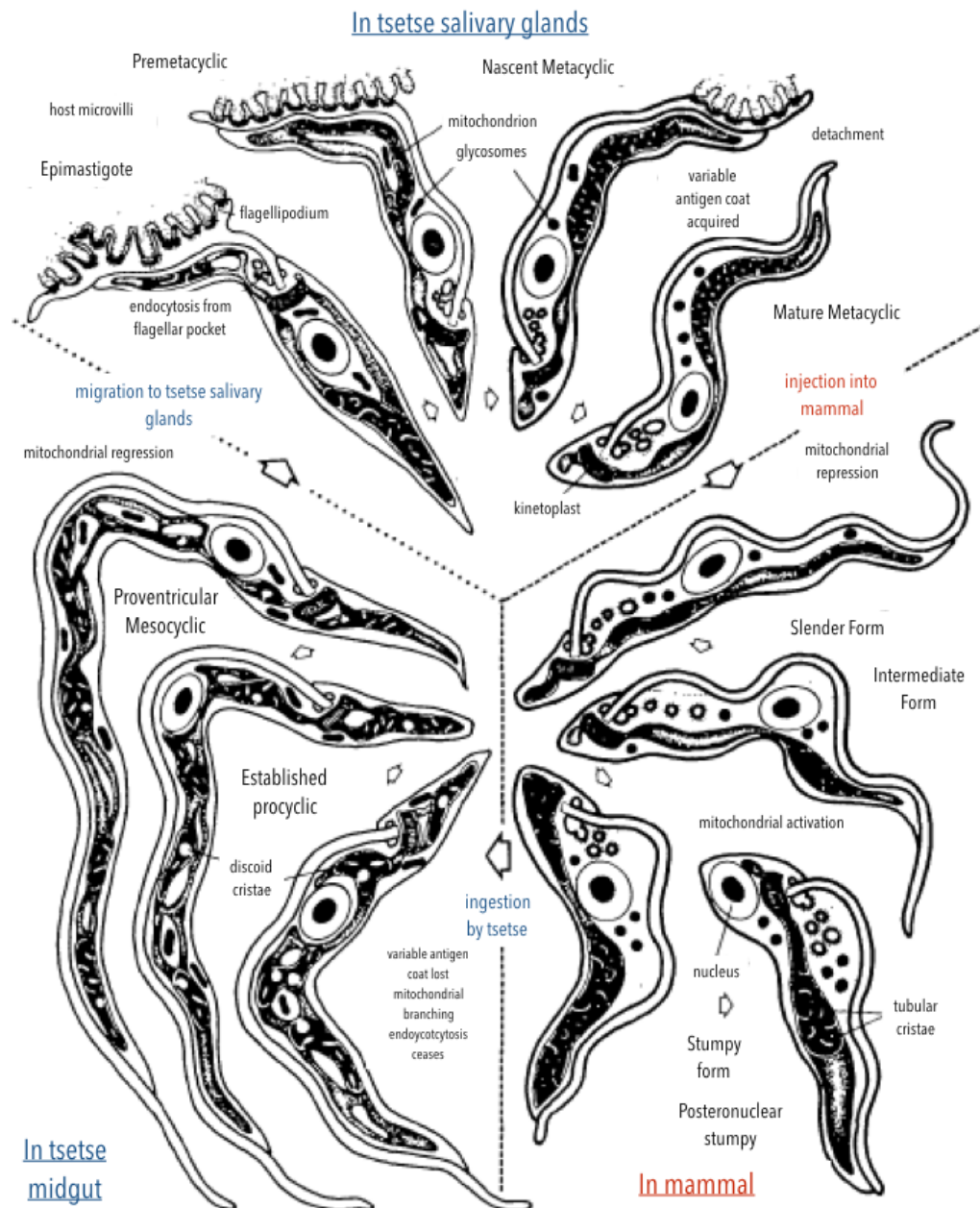


Figure 1.2. The developmental cycle of *Trypanosoma brucei* (adapted from Vickerman 1985)

The main developmental stages of *Trypanosoma brucei* in the mammal, in the tsetse midgut and the tsetse salivary glands are displayed. The changes of the surface coat, mitochondrion, glycosomes and endocytosis are indicated.

The ectoperitrophic trypanosomes are longer and as they move to the proventriculus their length further increases. The relative mitochondrial volume decreases. The proventricular mesocyclic trypanosomes establish an infection of the salivary glands and differentiate into epimastigote stage with a prenuclear kinetoplast. The epimastigote trypanosomes are able to

attach to the host microvilli of the epithelial cells lining the salivary glands lumen by the flagellar membrane flagellipodia³². Epimastigotes divide while attached, activate endocytosis and develop into premetacyclic trypanosomes, which have a postnuclear kinetoplast, retained the branched mitochondrion but their microvilli are reduced in size. Premetacyclic trypanosomes further develop into metacyclics, which cannot divide and acquired the VSG coat while still attached to the salivary gland surface. The mature metacyclics are preadapted for the injection and life in the mammalian host when the fly takes the next blood meal. By that the developmental cycle of the *T. brucei* parasite³³ is completed.

1.4 *Trypanosoma brucei* as a model organism

The group of trypanosomes branched off the eukaryotic tree very early during evolution. Thus, members of this group are a good model for studying not only the origin of parasitism (reviewed in³⁴) but also the conservation and divergence of genes and various biological processes within eukaryotes. The genome of *T. brucei*³⁵ as well as some other kinetoplastid species³⁶⁻³⁸ has been sequenced. Orthologs of many genes are conserved from trypanosomes to humans. An example is genes encoding flagellar proteins, which when deregulated in humans play a role in ciliopathy diseases. Such genes are currently studied in *T. brucei*³⁹.

The cellular architecture where most of the organelles are present in a single copy allows to study organelle duplication and segregation and the control of the cell division cycle⁴⁰

RNAi in *T. brucei*⁴¹ was discovered almost at the same time as in *Caenorhabditis elegans*⁴² and it opened a new avenue for reverse genetics. Currently other molecular tools such as recombination based gene deletion and *in situ* tagging⁴³ as well as inducible ectopic gene expression⁴⁴ are available (reviewed in⁴⁵).

The two most common axenic cultures of the parasite are the monomorphic mammalian LS BSF and tsetse fly PCF. Monomorphism in trypanosomes is a consequence of a prolonged cultivation in the cell culture, which results in the inability to fully respond to SIF. LS pleomorphic trypanosomes sustained the ability to respond to SIF and to differentiate to a stable PCF population. In contrast to monomorphic trypanosomes, pleomorphic strains are able to generate multiple waves of parasitemia in the infected animals. The ability

to differentiate enables the study of processes taking place during transition from one stage to another.

1.5 Host adaptation

During their life cycle, trypanosomes shuttle between the mammalian host and the tsetse fly vector, which are two completely different environments in terms of immune response challenges, energy resources and temperature. The parasite developed a sophisticated adaptation strategy and adjusted its morphology, metabolism, gene expression and organelle activity to survive and proliferate in these different host environments. Understanding the host adaptation of *T. brucei* during life cycle has been a challenging task in the field. Several genome-wide transcriptome analyses have been performed to elucidate how trypanosomes adapt to different host environments. In addition to the comparison of transcript abundance in PCF and BSF⁴⁶, transcriptomes of differentiating parasites were analyzed^{47, 48}. These groundbreaking studies provided many insights into the adaptation machinery of trypanosomes but there are certain limitations to transcriptome-based approaches. Due to the fact that the regulation of gene expression in trypanosomes occurs almost exclusively post-transcriptionally at the level of mRNA stability, translational efficiency and protein stability, the levels of mRNA do not always reflect the actual protein abundance in the cell⁴⁹. For example transcriptome-wide quantification of mRNA stability revealed that highly abundant transcripts in BSF have longer half lives compared to the same transcripts in PCF⁵⁰. Furthermore, translational efficiency in PCF and BSF varies greatly between these two life cycle stages as shown by ribosome profiling^{51, 52}. Hence, proteome-based studies are required to completely understand how the parasite changes during developmental differentiation. We therefore used stable isotope labeling (SILAC) to quantitatively compare the proteomes of BSF and PCF, which unraveled many new components of the host adaptation machinery⁵³. 4364 protein groups were analyzed in total and many new putative proteins of an unknown function were detected. 625 protein groups were enriched in PCF and 253 protein groups were enriched in BSF. Large-scale proteomic studies are extremely useful to approach cellular changes in a systematic way. However, to fully understand the functions and consequences of differential gene expression, detailed work on a molecular level is necessary. We therefore decided to characterize specifically putative proteins of unknown function that are highly upregulated in the BSF to learn more about novel

trypanosomal adaptation factors to the mammalian host. We hereby focused on a BSF specific putative flagellar protein Tb927.11.2400. Flagellar components are especially interesting because the flagellum is highly adapted to different host environments.

1.6 Flagellum of *Trypanosoma brucei*

Trypanosomes have a single flagellum attached along the cell body. The architecture of the flagellum (Fig. 1.3) has been reviewed previously^{54,55}. The flagellum emerges from the flagellar pocket (FP). The flagellar pocket membrane, the flagellum membrane and the cytoplasmic membrane of the cell body are distinct in composition. The FP is separated from the outer environment by a flagellar collar. The flagellum consists of a paracrystalline structure called the paraflagellar rod (PFR) and an axoneme. The axoneme is built by a canonical 9+2 arrangement of microtubules and it is anchored in the anterior of the cell by a barrel like structure called the basal body. The basal body is found in the cytoplasm and contains nine peripheral triplet microtubules without a central pair. As the basal body extends outwards, triplet microtubules become doublets and form the axoneme transition zone, which ends at the basal plate. The basal plate is the site where the central microtubules and thus axoneme begin. The flagellum attaches to the body all along the cell by a flagellar attachment zone (FAZ). The FAZ comprises a FAZ filament and a microtubule quartet, both associated with a flagellar endoplasmic reticulum. The composition of the flagellum has been revealed to a large extent by a proteomic study of the intact flagella in PCF⁵⁶. A growing body of evidence qualifies flagellum to be the major communication hub with the host environment providing sensing and response to extracellular signals. A combination of flagellum purification together with affinity purification of surface exposed proteins described flagellum matrix and surface proteins in BSF and gave an insight into flagellum signaling⁵⁷. Stage specific expression of individual paralogs within gene families was demonstrated by comparison of PCF and BSF cell surface proteomes, showing that the parasite surface is remodeled to allow adaptation to the different host environments⁵⁸. The flagellar membrane is in direct contact with the outer environment. In the tsetse fly it forms branched flagellar outgrowths while attached to the salivary gland epithelium⁵⁹.

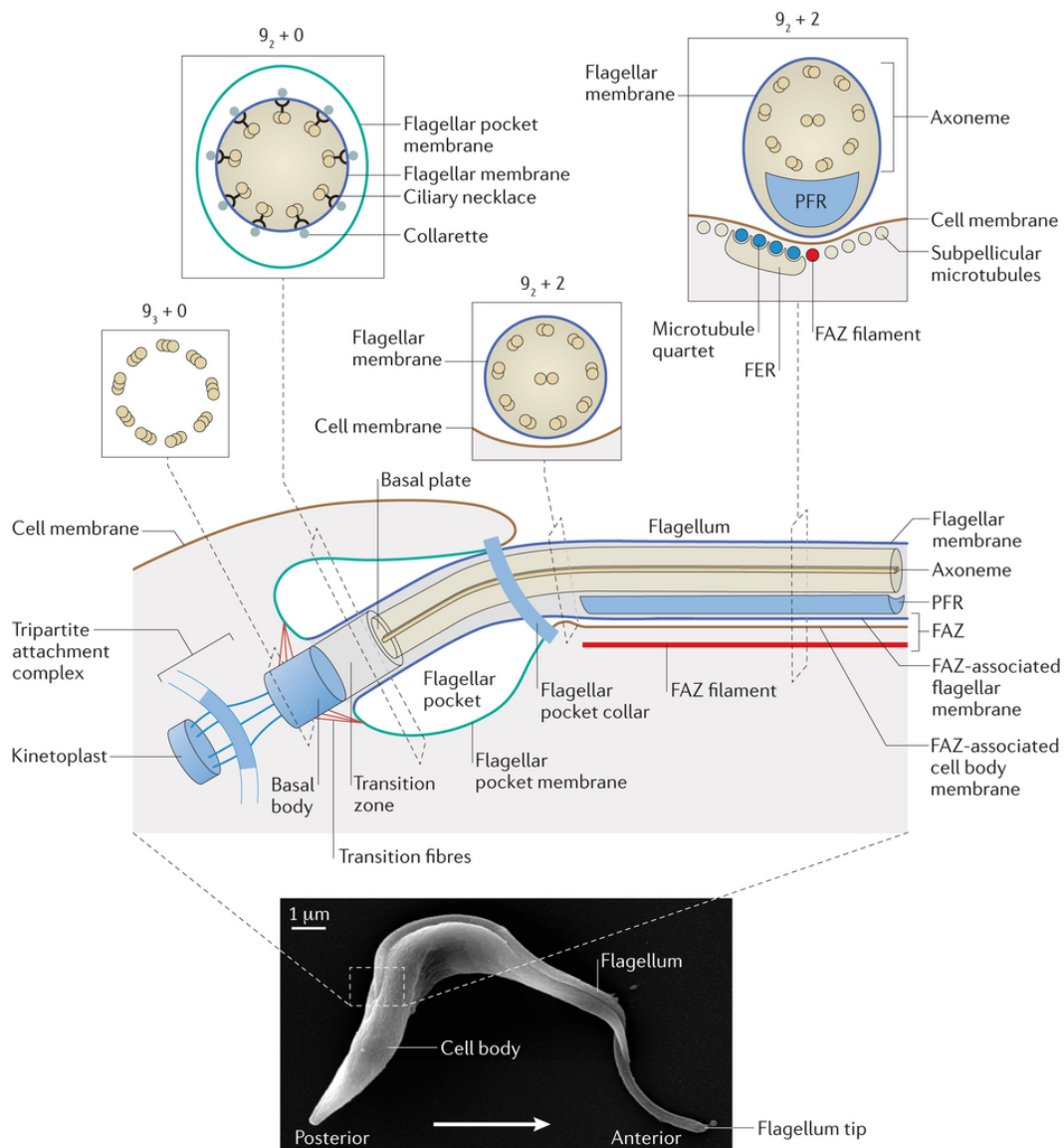


Figure 1.3. *T. brucei* flagellum (Figure from Langousis and Hill, 2014)

Scanning electron micrograph of *T. brucei* with the direction of movement of the cell indicated below. The square area is depicted in a cartoon above, where the flagellar pocket and a part of the flagellum are described in detail.

A recent study⁶⁰ reported a formation of membranous nanotubes, that originate from the flagellar membrane in BSF and dissociate into free extracellular vesicles (EVs). A proteomic analysis of isolated EVs revealed enrichment of flagellar proteins such as calflagin, adenylate cyclase (GRESAG4), glycoposphatidylinositol phospholipase C (GPI-PLC) and metacaspase 4 (MCA4). All of these proteins contribute to the virulence of *T. brucei* in the mammalian host⁶¹⁻⁶⁴. The EVs of *T. b. rhodensiense* contain a

serum resistance associated protein (SRA) necessary for human infectivity and they transfer SRAs to human non-infectious *T. b. brucei*. EVs fuse with mammalian erythrocytes and alter the properties of their membrane, which results in a rapid erythrocyte clearance and anemia⁶⁰. The flagellar membrane is enriched in raft forming lipids such as phosphatidylethanolamine, phosphatidylserine, ceramide and the sphingolipids inositol phosphorylceramide and sphingomyelin⁶⁵. The association of the flagellar calcium binding protein (FCaBP) with raft typical detergent domains in *T. cruzi*⁶⁶ indicates more ordered organization of the flagellar membrane. Another example is the group of PCF stage-specific flagellar surface receptor adenylate cyclases, which were shown to localize specifically to the flagellum tip. This supports subdomain organization of the flagellar membrane and a microdomain model for flagellar cyclic AMP (cAMP) signaling in *T. brucei*⁶⁷. Arginine kinase 3 (AK3) is highly expressed in PCF compared to BSF and was shown to confer advantage to the parasites during infection in tsetse flies. It is proposed to function as a phosphagen kinase involved in ATP buffering needed for the flagellar beat⁶⁸. Interestingly, AK3 shares similarity with the flagellar membrane targeting sequence of calflagins from *T. brucei* and flagellar calcium binding protein (FCaBP) from *T. cruzi*⁶⁸.

1.7 Aims of this thesis

The aim of this thesis was to characterize a candidate (Tb927.11.2400), identified previously in a SILAC based comparison of PCF and BSF proteomes, as a BSF-specific potential host adaptation factor. Database search revealed that Tb927.11.2400 shares 38% amino acid identity with PCF-specific *TbFlabarin* (Tb927.11.2410). We named Tb927.11.2400 *TbFlabarin-Like* (*TbFlabarinL*) following the convention adopted for Flabarins⁶⁹. Evolutionary analysis was carried out to understand the conservation of *TbFlabarinL* in trypanosomes. Polyclonal *TbFlabarinL* specific antibody was generated to localize this protein in the cell and to identify potential interacting partners in a co-immunoprecipitation experiment. To test if *TbFlabarinL* is an essential gene, it was depleted in the BSF trypanosomes using RNAi. It appeared to be dispensable for the normal growth of the cells in the cell culture. Thus *TbFlabarinL* was deleted in the pleomorphic trypanosomes via homologous recombination. To reveal a potential role of *TbFlabarinL* in the differentiation from BSF to PCF, the

$\Delta TbFlabarinL$ cell line was differentiated. Finally, to determine the localization of *TbFlabarinL* in the cell, BSF trypanosomes were biochemically fractionated.

2 Materials and methods

2.1 Computational analyses

A BLAST search with *TbFlabarinL* (Tb927.11.2400) was performed using the TriTryp database⁷⁰. Alignments were obtained from constraint-based multiple alignment tool (COBALT)⁷¹ at the NCBI database and edited in Esprout 3.0⁷². Protein structures of *TbFlabarinL* and *TbFlabarin* were predicted by the Phyre2 server⁷³ and edited in UCSF Chimera 1.10.2⁷⁴. Datasets for phylogenetic analyses were received from publicly available sources (Tab 2.1) for both *Flabarin* and *FlabarinL* genes, using BLASTP at an E-value cut-off of 10⁻²⁰. All amino acid sequences were searched for conserved domains by Pfam. The datasets were aligned by MUSCLE and relevant positions were selected using Gblocks. Phylogenetic model selection with Model generator favored LG+GAMMA model and ML trees were constructed using RAxML 8.1.17 with 1 000 bootstrap replicates. Bayesian Monte Carlo Markov (MCM) chain analysis was performed with GTR+GAMMA+CAT model using Phylobayes 3.3f running 8 independent chains for 10,000 cycles. Convergence of chains was estimated by comparison of bipartition frequencies in individual chains, discarding first 2,000 cycles. *

* Tomas Skalicky carried out the evolutionary analyses.

2.2 Molecular cloning

2.2.1 DNA fragments amplification

DNA fragments were amplified by PCR using Phusion high fidelity polymerase reagent set (Thermo Fisher Scientific) according to the manufacturer's instructions. All oligonucleotides (Tab 2.2) were synthesized by Sigma-Aldrich. Trypanosome genomic DNA (200 ng) or plasmid DNA (10 ng) was used as a DNA template. Cycling conditions were adjusted to the specific primer pair and the template length and either a 3 step PCR program: 98°C 2 min - (98°C 30 s, X°C 30 s, 72°C 30s/kb) x 28 cycles - 72°C 5 min or a 2 step PCR program: 98°C 2 min - (98°C 30 s, 72°C 30s/kb) x 28 cycles - 72°C 5 min was used.

2.2.2 Fragmentation of DNA molecules by restriction endonucleases

DNA molecules were digested using commercial restriction endonucleases (New England Biolabs or Thermo Fisher Scientific) to linearize plasmids or to

obtain fragments with the required nucleotide overhangs. 20 or 2 µg of DNA were digested in 30 – 50 µl reaction according to the manufacturer's instructions.

2.2.3 Separation and isolation of DNA fragments

DNA fragments were separated according to the size by an agarose gel electrophoresis. Agarose gels contained 0.75 % Agarose in TAE buffer (40 mM tris/hydrochloric acid (HCl) pH 8.0; 20mM acetic acid; 1 mM ethylenediaminetetraacetic acid (EDTA)) and 0.1 µg/ml ethidium bromide to stain the DNA. DNA samples were mixed with DNA loading dye (Thermo Fisher Scientific) and Gene Ruler ladder mix (Thermo Fisher Scientific) was used for fragment size estimation. Separation of DNA molecules was performed in Tris-acetate-EDTA (TAE) buffer at current voltage of 120 V for 30 min. DNA was visualized by UV light on Gel iX Imager (Intas). Separated DNA fragments were excised from gel under UV illumination (Vilber Lourmat) and purified using Gel and PCR extraction kit (Macherey Nagel) according to the manufacturer's protocol. The concentration of purified DNA was quantified by Infinite M200 Reader (Tecan).

2.2.4 Ligation of DNA fragments

DNA fragments were ligated into plasmids in 20 µl volume using DNA ligase (Thermo Fisher Scientific) according to the manufacturer's instructions at 4°C over night.

2.2.5 Transformation of chemically competent *Escherichia coli*

10 µl of the ligation reaction (or 1 ng plasmid for amplification) was added to the chemically competent *E. coli* (Tab. 2.3) and incubated on ice for 15 min prior to a 45 s heat shock at 42°C and a subsequent 2 min incubation on ice. 500 µl of superoptimal broth with catabolite repression (SOC) media (2% tryptone, 0.5% yeast extract, 10 mM NaCl, 2.5 mM KCl, 10 mM MgCl₂, 10 mM MgSO₄, and 20 mM glucose) was added and bacteria were incubated at 200 rpm, 45 min at 37°C. Bacteria were sedimented (3000 x g, 1 min, RT) supernatant removed leaving 30 µl in the tube. The pellet was resuspended in the remaining volume and plated on Luria Bertani (LB) agar plates (0.5 % yeast extract, 1% bacto tryptone, 1% NaCl, pH 7.5, 1.5% agarose) supplemented with an appropriate antibiotic (100 µg/ml ampicilin or 34 µg/ml chloramphenicol) for selection.

2.2.6 Growth of *E. coli*

E. coli were grown at 37°C, 200 rpm over night in liquid LB media (0.5 % yeast extract, 1% bacto tryptone, 1% NaCl, pH 7.5) or on LB agar plates supplemented with an appropriate antibiotic (100 µg/ml ampicilin or 34 µg/ml chloramphenicol) for selection.

2.2.7 Isolation of plasmid DNA from *E. coli*

Plasmid DNA was isolated from 2 ml or 100 ml of overnight bacterial culture using miniprep NucleoSpin plasmid (Macherey Nagel) or midiprep Nucleobond 100 (Macherey Nagel) kit according to the instructions of the manufacturer.

2.2.8 Purification of DNA

DNA was purified after PCR either directly or from agarose gel using the NucleoSpin gel and PCR cleanup kit (Macherey Nagel) according to the manufacturer's instructions. Alternatively, DNA was precipitated using isopropanol – sodium acetate method. One volume of isopropanol and 0.1 volume of sodium acetate (3M pH 5.2 stock) was added to one volume of DNA, mixed and incubated in -20°C for 40 min or over night. DNA was sedimented at 21 000 x g, 4°C for 30 min. DNA pellet was washed 2x in 500 µl of 70% ethanol (21 000 x g, 10 min, 4°C), supernatant removed and pellet dried and dissolved in water.

2.2.9 Purification of *T. brucei* genomic DNA

Genomic DNA of *T. brucei* was purified using High Pure PCR Template Preparation kit (Roche). Briefly, 5×10^6 cells were harvested (1500 x g, 10 min, RT) and pellet was dissolved in phosphate saline buffer (PBS) (10 mM Na₂HPO₄, 1.8 mM KH₂PO₄ pH 7.4, 140 mM NaCl, 2.7 mM KCl) and 200 µl Binding Buffer, 40 µl Proteinase K, mixed and incubated at 70°C for 10 min. 100 µl of isopropanol was added, mixed, DNA bound onto a column (8000 x g, 1 min, RT) and washed first with 500 µl of Inhibitor removal buffer (8000 x g, 1 min, RT) and second with 500 µl of Wash buffer (8000 x g, 1 min, RT). Prior to DNA elution, column was dried (21 000 x g, 1min, RT). DNA was eluted with 200 µl of Elution buffer.

2.3 Sodium dodecyl sulfate polyacrylamide gel electrophoresis (SDS-PAGE)

SDS-PAGE was used to separate proteins according to their molecular mass. Gels were handcasted, the separating gel contained 10% acrylamide/bisacrylamide (29:1) in separating gel buffer (1.5 M Tris/HCl pH 8.8, 0.4% (w/v) SDS) and stacking gel 5% acrylamide/bisacrylamide (29:1) in stacking gel buffer (500 mM Tris/HCl pH 6.8, 0.4% (w/v) SDS). Protein samples were prepared in 2x Laemmli sample buffer (166 mM Tris HCl, 3.3% SDS, 10% glycerol, 0.3 M DTT, 0.012% bromphenol blue, pH 6.8) with a final concentration of 2×10^5 cells/ μ l in case of trypanosomes and 5×10^6 cells/ μ l in case of *E.coli*, loaded into the gel chamber (Bio-Rad) along with PageRuler prestained protein marker (Thermo Fisher Scientific) for the size estimation. Electrophoresis was performed at 180 V using electrophoresis power supply EV265 Consort (Hoefer, Inc.).

2.4 Western blot

Whole cell lysates were separated by 10% SDS-PAGE and transferred onto an Immobilon® PVDF membrane (MERCK MILLIPORE) activated in methanol for 10 s and soaked in water. Blotting sandwich was assembled (bottom to top) from two thick Whatman papers soaked in anode buffer (25 mM Tris/HCl pH 7.6, 20% (v/v) methanol), SDS-PAGE, membrane and one thick Whatman paper soaked in cathode buffer (300 mM Tris/HCl pH 7.6, 20% (v/v) methanol, 40 mM epsilon-aminocaproic acid). Proteins were transferred in a semi-dry blotter (Bio-Rad) at 54 mA/gel at maximum voltage set to 25 V for 1 h using electrophoresis power supply EV265 Consort (Hoefer, Inc.). To block unspecific binding of the antibodies, the membrane was incubated in PBS-5% milk for at least 1 h prior to the incubation with primary antibodies (Tab 2.6) in PBS-0.1% Tween, 1% milk for 1 h at RT followed by 3 wash steps in PBS-0.2% Tween for 10 min. Polyclonal anti-*Tb*FlabarinL rabbit antibody generated in this study was diluted 1:500. Monoclonal anti-PFR mouse antibody L13D6, monoclonal anti-tubulin TAT1 and BB2 anti-TY mouse antibodies were gifts from K. Gull (University of Oxford) and described elsewhere^{75, 76,77}. Anti-*Tb*MORN1 rabbit antibody was kindly provided by Brooke Morriswood (University of Würzburg)⁷⁸. Polyclonal *Tb*FlabarinL specific rabbit antibody was generated in this study (Tab. 2.6). To visualize the respective proteins, membrane was incubated with secondary antibodies IRDye680 and/or IRDye800 coupled anti-mouse or

anti-rabbit (LI-COR Bioscience) diluted 1: 20 000 in PBS-0.1% Tween with 1% milk and 0.02% SDS 1 h at RT and detected with Odyssey infrared imaging system (LI-COR Bioscience).

2.5 Cultivation and transfection of trypanosomes

Monomorphic BSF trypanosome Single Marker (SM) line and PCF line are both derivative from Lister strain 427, antigenic type MiTat 1.2, clone 221a (Doyle et al., 1980) and express T7 polymerase and Tetracycline repressor⁴⁴. Monomorphic BSF trypanosome 2T1 line is a derivative from Lister strain 427, antigenic type MiTat 1.2, clone 221a and is engineered to express TetR⁷⁹ and to contain a landing pad within a ribosomal spacer on chromosome 2a, consisting of a 3'-hygromycin phosphotransferase (*HYG*) fragment and *VSG* expression site promoter-driven puromycin N-acetyltransferase (*PAC*) open reading frame (ORF)⁸⁰. Monomorphic BSF trypanosomes were maintained in HMI-9 medium⁸¹ modified by Vassella⁸². Briefly, 17.66 g Iscove's modified Dulbecco's MEM (IMDM) powder were dissolved in 1 l double distilled water, pH was adjusted to 7.5 and medium was complemented with 3.024 g sodium bicarbonate, 136 mg hypoxanthine, 28.2 mg bathocuproine sulfonate, 14 µl β-mercaptoethanol, 39 mg thymidine, 100.000 U penicillin, 100 mg streptomycin, 182 mg cysteine and 10% (v/v) of heat inactivated (1 h, 56°C) fetal calf serum (FCS) and subsequently sterilized by filtration (pore size 0.2 µm). PCF trypanosomes were cultured in modified SDM-79 medium⁸³. BSF and PCF cell densities were determined using particle Coulter Counter Z2 (Beckman Coulter) and cultures diluted to maintain the mid log growth phase. Monomorphic trypanosomes transfections were performed as described previously⁸⁴. 1×10^7 BSF cells were harvested (1500 x g, 10 min, RT) and pellet washed in pre-warmed trypanosome dilution buffer (TDB) (5 mM KCl, 80 mM NaCl, 1 mM MgSO₄, 20 mM Na₂HPO₄, 2 mM NaH₂PO₄, 20 mM glucose, pH 7.4) (1500 x g, 10 min, RT). Cell pellet was dissolved in 400 µl of transfection buffer (90 mM Na₂PO₄, 5 mM KCl, 0.15 mM CaCl₂, 50 mM HEPES, pH 7.3) and 10 µl of DNA (1 µg/µl) were added and transferred into the BTX cuvette and electroporated using AMAXA nucleofector (Lonza) and program X-001 free choice. Cells were transferred into 50 ml of pre-warmed HMI9 medium and 1:10 dilution was plated on two 24 well plate (1 ml/well). Selective drugs were added in medium (1 ml/well) in the double concentration 6-8 h post transfection. 1×10^7 PCF cells were harvested (1500 x g, 10 min, RT) and

pellet washed in PBS (1500 x g, 10 min, RT). Cell pellet was dissolved in 400 μ l of transfection buffer and 10 μ l of DNA (1 μ g/ μ l) were added and transferred into the BTX cuvette and electroporated as in the case of BSF. Cells were transferred into 30 ml of SDM79 medium supplemented with 20% of conditioned SDM79 medium (prepared by growth of PCF in the medium, sedimentation of the cells (1500 x g, 10 min, RT) and filtration of the supernatant through 0.2 μ m filter). 1:10, 1:100 and 1:1000 dilutions were plated on 24 well plates (1 ml/well). Selective drugs were added in medium (1 ml/well) in the double concentration 14 h post transfection. Pleomorphic BSF trypanosomes AnTat1.1 were cultured in HMI-9 medium containing 1.1% methylcellulose. Cell density was determined using Neubauer counting chamber (Brand) and cultures diluted to maintain the density of 3×10^5 cells/ml. Cells were transfected as described previously^{85, 86}. Briefly, 150 ml cell culture at a density of at least 3×10^5 cells/ml cells was diluted 1:5 in TDB and filtered using a reusable bottle top filter holder (Nalgene) with a round filter 615 (Macherey Nagel) to remove most of the methyl cellulose. Cells were sedimented by centrifugation (1500 x g, 10 min, 37°C) and pellet washed with 1 ml of TDB and used for transfection as described previously⁸⁶. Cell pellet was dissolved in 100 μ l of basic parasite nucleofector solution 2 (Lonza) and 15 μ l of DNA (1 μ g/ μ l) were added and transferred into the AMAXA cuvette and electroporated using AMAXA nucleofector (Lonza) and program X-001 Mouse CD8+ T cells. Cells were transferred into 5 ml of pre-warmed HMI9 and 35 ml of methylcellulose media were added. Undiluted pool, 1:5 and 1:10 dilutions were plated on 24 well plates (1 ml/well). Selective drugs were added in HMI-9 medium containing 1.1% methylcellulose (1 ml/well) in the double concentration 6-8 h post transfection.

2.6 Differentiation of trypanosomes

Pleomorphic AnTat1.1 BSF were grown to a density of 2.5×10^6 cells/ml, diluted 1:5 in TDB, filtered, sedimented by centrifugation (1500 x g, 10 min, 37°C) and resuspended to a cell density of 2×10^6 cells/ml in DTM medium⁸⁷. A mixture of cis-aconitate and isocitrate (3 mM) was added to induce differentiation and cells were incubated at 27°C with 5% CO₂⁸⁷.

2.7 Generation of transgenic trypanosome cell lines (Tab. 2.5)

To generate the *TbFlabarinL*^{RNAi} cell line, a DNA fragment (positions 30 - 544 nt) was PCR amplified from genomic DNA using forward primer containing *Sma*I and *Xho*I restriction sites and reverse primer containing *Bam*HI and *Xba*I sites. Sense and antisense fragments of the RNAi hairpin were cloned into pRPAiSL vector⁸⁸. Prior transfection into 2T1 cells, the plasmids were linearized using *Asc*I. Clones with a correctly integrated construct were selected as described previously⁸⁸. RNAi was induced by addition of 1 µg/ml tetracycline to the cell culture.

A PCR based gene deletion approach was used to sequentially replace both alleles of *TbFlabarinL* by *HYG* and *PAC* ORFs in MiTat1.2 SM. The *TbFlabarinL* 5' UTR (59 nt) and 3' UTR (60 nt) were flanked by sequences to amplify *HYG* and *PAC* ORFs from the pHD309 *HYG/PAC* plasmid (gift from G.A.M. Cross). Cells were electroporated with the precipitated PCR products. The same constructs were used to delete both *TbFlabarinL* alleles in AnTat1.1 pleomorphic strain. Correct integration of the constructs was verified by PCR using primers binding in the 5' and 3'UTR, at the 5' and 3' ends of the *TbFlabarinL* ORF and within the *PAC* and *HYG* ORFs. PCR was performed according to the manufacturer's instructions of the Phusion Human Specimen Direct PCR Kit (Thermo Fisher Scientific) with minor modifications. 1x10⁶ cells were sedimented by centrifugation (1500 x g, 10 min, RT) and cell pellet was resuspended in 20 µl Dilution buffer. 0.5 µl DNA release was added and samples were incubated 5 min at RT followed by 2 min at 98°C. Samples were sedimented by centrifugation (2000 x g, 5 min, RT) and 0.5 µl of the supernatant was used as template in a 20 µl PCR reaction.

TbFlabarinL was epitope tagged at the N- or C-terminus in the endogenous locus as described previously⁴³. The plasmids for tagging were kindly provided by S. Kramer (University of Würzburg). Briefly, the *TbFlabarinL* fragment (positions 1-607 nt) was amplified from genomic DNA and cloned into p3077_*PAC*_4xTY plasmid. The vector was linearized within the ORF fragment by *Hpa*I prior to transfection of the cells. To tag *TbFlabarinL* at the C-terminus, a part of the *TbFlabarinL* ORF (positions 2-653 nt) was amplified from genomic DNA and cloned into p3074_4xTY_*BLE* plasmid and linearized by *Hpa*I before transfection of the cells. The same strategy was used to tag *TbFlabarin* (Tb927.11.2410) at the C-terminus. A fragment of the *TbFlabarin* ORF (positions 1-666 nt) was cloned into p3074_4xTY_*BLE* plasmid and linearized with *Bcl*I enzyme prior to transfection. To tag PAR1

(Tb927.11.13500) at the N-terminus, a fragment (positions 4-823 nt) of PAR1 ORF was cloned into the p3077_PAC_4xTY plasmid and EcoRI enzyme was used for linearization.

To express *TbFlabarinL* in PCF ectopically, its ORF was amplified from genomic DNA and cloned into pLEW100v5b2x_BLE (gift from G.A.M. Cross) using XhoI and HindIII restriction sites. For ectopic expression of *TbFlabarin* in BSF, the *TbFlabarin* ORF was amplified from genomic DNA using C-terminal primer containing a glycine-alanine-glycine (Gly-Ala-Gly) linker sequence followed by a TY tag sequence and cloned into pLEW100v5b2x_BLE using XhoI and HindIII restriction sites. Constructs were linearized with NotI for integration into the ribosomal spacer locus. Expression was induced by addition of 1 µg/ml tetracycline to the cell culture.

2.8 Polyclonal Antibody Generation

The *TbFlabarinL* ORF was amplified from genomic DNA of *T. brucei* using a primer containing 10 x His tag sequence and a Gly-Ala-Gly linker sequence and cloned into pETDUET-1 vector (Novagen) using NcoI and XhoI restriction sites. *TbFlabarinL* was expressed in Rosetta Blue *Escherichia coli* (Tab. 2) according to the manufacturers instructions. Protein test expression and solubility test and purification were performed according to the guidelines of the NiNTA Agarose manufacturer (Qiagen) used to nickel-affinity purify recombinant *TbFlabarinL* in a small scale. To obtain enough protein for antibody generation, expression was scaled up and purification performed by Äkta prime plus system (GE Healthcare) using a HisTrap FF crude 1 ml column (GE Healthcare). 800 ml of pre-warmed LB media supplemented with 100 µg/ml ampicillin, 34 µg/ml chloramphenicol and 1% glucose was inoculated with an overnight bacterial culture to optical density at 600 nm (OD₆₀₀) of 0.1 and incubated at 37°C, 200 rpm till OD₆₀₀ of 0.5 was reached. OD₆₀₀ was measured using a spectrophotometer (Eppendorf). *TbFlabarinL* expression was induced with 1 mM IPTG for 3 h at 37°C, 200 rpm. Bacterial culture was sedimented (10 000 x g, 10 min, 4°C). Bacteria were lysed in 10 ml lysis buffer (50 mM NaH₂PO₄ pH 8.0, 300 mM NaCl, 10 mM imidazole, 1% Triton X-100) supplemented with Complete protease inhibitor cocktail without EDTA (Roche) by sonication using Bioruptor (Diagenode) with a setting of 10 cycles 30 s high power pulse with 30 s pause. Lysates were sedimented (21 000 x g, 20 min, 4°C) and supernatant filtered through a 0.45

µm filter and diluted in 3.5 ml of binding buffer (50 mM NaH₂PO₄, 300 mM NaCl, 20 mM imidazole, pH 7.4). Filtrate was injected into the Äkta prime sample loop and a manual run (Tab. 2.5) started. Fraction samples from the purification process were separated by 10% SDS-PAGE and proteins visualized by Coomassie staining. SDS-PAGE was boiled in water for 1 min in microwave, water discarded and gel stained with Coomassie solution (0.02% Coomassie brilliant blue G-250, 5% aluminium sulfate-(14-18)-hydrate, 10% ethanol, 2% orthophosphoric acid) for at least 30 min and washed with water prior to scanning with Odyssey infrared imaging system (LICOR Bioscience). Fractions containing recombinant *TbFlabarinL* were pooled, dialyzed and concentrated using a centrifugal filter unit with a 10 kDa cut off (Amicon). Protein concentration was determined via Bradford assay using solution for protein determination (Applichem) according to the manufacturer's instructions. 500 µg of purified protein was sent to Pineda (Berlin) for antibody production. *TbFlabarinL* specific antibody was affinity purified from the rabbit immune sera using the SulfoLink kit (Thermo Fisher Scientific) according to the manufacturer's instructions. Briefly, 1 mg of purified recombinant *TbFlabarinL* was immobilized onto 0.5 ml SulfoLink resin. *TbFlabarinL* specific antibody was purified from 5 ml of immune sera. Antibody specificity was tested in WB using recombinant *TbFlabarinL* and whole lysates of BSF, PCF, Δ *TbFlabarinL* and *TbFlabarinL*^{RNAi} cell lines.

2.9 Immunofluorescence (IF)

1x10⁷ cells were harvested by centrifugation (1500 x g, 10 min, RT) and resuspended in 1 ml TDB. Cells were fixed in 2% PFA (10 min, RT). After 3 wash steps in PBS, cells were settled onto Poly-L-lysine coated slides for 20 min and permeabilized 5 min in 0.2% NP-40 in PBS. Unspecific epitopes were blocked with 1% BSA in PBS for 1 hr at 37°C. Cells were incubated with the primary *TbFlabarinL* antibody (diluted 1:200 in PBS-0.1% BSA) and/or monoclonal BB2 anti-TY mouse antibody and/or TAT1 mouse anti-tubulin antibody (Tab. 2.6) at RT for 1 hr. After washing, the secondary antibody was applied (Alexa 594 anti-mouse, Alexa 488 anti-rabbit (Life Technologies)) for 30 min at RT. DNA was stained with 1 µg/ml 4,6-diamidino-2-phenylindole (DAPI) and cells were embedded in ProLong Gold Antifade (Molecular Probes) and imaged on Leica DMI 6000B microscope. Images were processed using Huygens Essential XII deconvolution software (Scientific Volume Imaging).

2.10 Co-immunoprecipitation

Polyclonal *Tb*FlabarinL specific antibody was immobilized to protein G Sepharose Fast Flow beads (GE Healthcare). Non-specific binding was blocked with 0.5% BSA in 20 mM sodium phosphate buffer pH 7.0. Four biological replicates per cell line (2×10^8 cells each) were harvested by centrifugation ($1500 \times g$ 10 min, 4°C) and washed in TDB buffer. Cells were lysed in 400 μl IP buffer (150 mM NaCl, 20 mM Tris HCl pH 8, 10 mM MgCl_2 , 0.25 % NP-40, 1 mM DTT, Complete protease inhibitor cocktail without EDTA (Roche)) by sonication using a Bioruptor (Diagenode) with a 3 cycles 30s high power pulse and 30 s pause setting. Cell lysates were incubated with the blocked beads (orbital mixing, overnight, 4°C). Beads were washed 2x in IP buffer (5 min on ice, centrifugation $1000 \times g$, 10 min, 4°C). To elute the proteins, beads were resuspended in 65 μl NuPAGE LDS Sample Buffer (Novex, Life Technologies) supplemented with 100 mM DTT and incubated 10 min at 70°C . The eluates were analyzed by mass spectrometry.

2.11 Mass Spectrometry **

Protein samples were separated on a 4-12% NuPAGE Gel (Life Technologies), and stained with Coomassie colloidal blue (Life Technologies). The lanes were sliced and prepared by in-gel digestion with trypsin⁸⁹. The peptides were stored on StageTips. Digested peptides were separated on a C18 reverse phase column (packed in-house, 20 cm, 75 μm inner diameter; packed with repositilPur-1.8 [Dr. Maisch]) with a 105-minute gradient from 5 to 95 percent ACN on an Easy-nLC 1000. The solution was directly sprayed at 2.4 kV. The Q Exactive Plus was operated in a data-dependent Top10 acquisition mode with one full scan (70,000 resolution, max injection 20 ms, 300-1650 m/z) and up to 10 HCD fragment scans (17,500 resolution, max injection 120 ms). The raw spectra were analyzed with MaxQuant ver1.5.1.0⁹⁰ using standard settings (except activated LFQ quantitation and match between runs) and the *Trypanosoma brucei* TriTrypDB-8.0_TbruceiTREU927 database.

2.12 Statistical analysis **

The protein groups file was filtered to exclude contaminants, reverse entries and proteins only identified by site prior to statistical analysis. To obtain enrichment the LFQ values were log₂ transformed and the mean between

bait and control was calculated. To assess statistical significance of the enrichment a Welch t-test for LFQ values between bait and control set was performed. Both values were visualized in a volcano plot using the ggplot2 package in R.

**Falk Butter performed the mass spectrometry and statistical analyses.

2.13 Isolation of cytoskeletons and flagella

Cytoskeletons were extracted and flagella isolated as described elsewhere^{84, 85} with minor modifications. Briefly, 1×10^8 were harvested by centrifugation (1500 x g, 10 min, 4°C) and washed in 1 ml PEME buffer (2 mM EGTA, 1 mM MgSO₄, 0.1 mM EDTA, 0.1 M piperazine-N,N'-bis (2-ethanesulfonic acid)-NaOH (PIPES-NaOH), pH 6.9). Cytoskeletons were detergent extracted in PEME buffer supplemented with 1% NP-40 for 15 min at RT under orbital mixing. Flagella were isolated by incubation of the extracted cytoskeletons in PEME buffer supplemented with 1% NP-40 and 1M KCl for 30 min at RT under orbital mixing. All solutions were supplemented with Complete protease inhibitor cocktail without EDTA (Roche). Samples obtained during the isolation steps were further analyzed in WB.

2.14 Chemicals

Most of the chemicals used in this study were purchased from Sigma-Aldrich, AppliChem and Roth if not stated otherwise.

Table 2.1. List of proteins used for phylogenetic analysis

Organism	Ortholog	Accession number
<i>T. brucei brucei</i>	<i>TbFlabarin</i>	Tb927.11.2410
<i>T. brucei gambiense</i>	<i>TbFlabarin</i>	Tbg927.11.2210
<i>T. congolense</i>	<i>TbFlabarin</i>	TcIL3000.11.2210
<i>T. cruzi</i> Dm28c	<i>TbFlabarin</i>	ESS66808.1
<i>T. cruzi</i> CL Brener	<i>TbFlabarin</i>	TcCLB.506125.20
<i>T. equiperdum</i>	<i>TbFlabarin</i>	CZPT01000935.1
<i>T. grayi</i>	<i>TbFlabarin</i>	XP_009315916.1
<i>T. vivax</i>	<i>TbFlabarin</i>	TvY486_0013090
<i>L. panamensis</i>	<i>TbFlabarin</i>	XP_010700258.1
<i>L. braziliensis</i>	<i>TbFlabarin</i>	XP_001565941.1
<i>L. mexicana</i>	<i>TbFlabarin</i>	XP_003876746.1
<i>L. infantum</i>	<i>TbFlabarin</i>	XP_001466397.1
<i>L. major</i> Friedlin	<i>TbFlabarin</i>	XP_003721979.1
<i>L. seymouri</i>	<i>TbFlabarin</i>	KPI89862.1
<i>L. pyrrhocoris</i>	<i>TbFlabarin</i>	H10_07_2100
<i>A. deanei</i>	<i>TbFlabarin</i>	EPY38881.1
<i>C. fasciculata</i>	<i>TbFlabarin</i>	CFAC1_230031800
<i>L. donovani</i>	<i>TbFlabarin</i>	LdBPK_271630.1
<i>L. tarentolae</i>	<i>TbFlabarin</i>	P27.1790
<i>L. tropica</i>	<i>TbFlabarin</i>	LTRL590_270024000
<i>T. evansi</i>	<i>TbFlabarin</i>	TevSTIB805.11.01.2480
<i>Phytomonas</i> sp. EM1	<i>TbFlabarin</i>	CCW60919.1
<i>Phytomonas</i> sp. Hart1	<i>TbFlabarin</i>	CCW71432.1
<i>E. monterogeii</i>	<i>TbFlabarin</i>	EMOLV88_270021800
<i>P. confusum</i>	<i>TbFlabarin</i>	KU375192
<i>C. acanthocephali</i>	<i>TbFlabarin</i>	AUXI01000516.1
<i>H. muscarum</i>	<i>TbFlabarin</i>	AUXJ01000865.1
<i>S. galati</i>	<i>TbFlabarin</i>	AUXN01000492.1
<i>S. oncopelti</i>	<i>TbFlabarin</i>	AUXK01006077.1
<i>A. desouzai</i>	<i>TbFlabarin</i>	AUXL01001281.1
<i>S. culicis</i>	<i>TbFlabarin</i>	AUXH01000047.1
<i>T. brucei brucei</i>	<i>TbFlabarinL</i>	Tb927.11.2400
<i>T. brucei gambiense</i>	<i>TbFlabarinL</i>	Tbg972.11.2650
<i>T. vivax</i>	<i>TbFlabarinL</i>	TvY486_1102400
<i>T. evansi</i>	<i>TbFlabarinL</i>	TevSTIB805.11.01.2450

Table 2.2. Primers

Primer	Fw/Rv	Sequence 5'-3'	Application
ZC37	Fw	GAGAAAGCCTTGGCGACAG	integration PCR (check of TbFlabarinL deletion)
ZC38	Rv	CAGTTCTCCGTCGCCACGTC	integration PCR (check of TbFlabarinL deletion)
ZC83	Fw	CCG GAA TTC AAG CTT CCG CCA CCATGGGTGGCGGTCCAAACCTAAC	N-terminal tagging of TbFlabarinL with 4xTY <i>in situ</i>
ZC84	Rv	CCGCAGTAGAAGGCGTATCGGTAAG	N-terminal tagging of TbFlabarinL with 4xTY <i>in situ</i>
ZC96	Fw	CCCGGGCTCGAGGTTAAGCAGAGATGGAGGAAAGG	RNAi of TbFlabarinL
ZC97	Rv	GATCGAATTCGGATCCTVAGAGCTTCCACCAACGTCAGGAAAC	RNAi of TbFlabarinL
ZC101	Fw	CCGGAATCCCATGATAGCCACCACCACCACCACCACCACCGGGGTTGGCGGTTCCAAACC TAACG	10x N terminally His tagged TbFlabarinL-recombinant protein production
ZC102	Rv	CCGGAATCCCGATTACTCGGATTTGTAICTCTGGAGACTATTCACC	10x N terminally His tagged TbFlabarinL-recombinant protein production
ZC120	Fw	GTCATATAAGCGTTGATCCCAAAAGTAATAACAGTAAGAAACATAAAGATATATCATATGACCGAGTACACGCCACG	deletion of TbFlabarinL replacement of allele by PAC ORF; flanked by endogenous UTRs
ZC121	Rv	CCTTTTATGCGCTGTGAAAACTGCATCTTAAGTCCATGTTCTGCTCAITGGCTAATAGGACCCGGGCTTGGCGG	deletion of TbFlabarinL replacement of allele by PAC ORF; flanked by endogenous UTRs
ZC122	Fw	GTCATATAAGCGTTGATCCCAAAAGTAATAACAGTAAGAAACATAAAGATATATCATATGAAAAAGCCTGAACCTACCGCG	deletion of TbFlabarinL replacement of allele by HYG ORF; flanked by endogenous UTRs
ZC123	Rv	CCTTTTATGCGCTGTGAAAACTGCATCTTAAGTCCATGTTCTGCTCAITGGCTAATAGGACCCGGGACGAG	deletion of TbFlabarinL replacement of allele by HYG ORF; flanked by endogenous UTRs
ZC124	Fw	TGCAAGACCTGCCCTGAAACC	binds in HYG ORF; integration PCR
ZC127	Fw	ATGGGTTGGCGGTTCCAAACC	integration PCR (check of TbFlabarinL deletion)
ZC128	Rv	CTCGGATTTGACTCTGGAGACTATTCACC	integration PCR (check of TbFlabarinL deletion)
ZC129	Fw	CCGGAATCCCAAGCTTATGGTTGGGTTCCAAACCTAAGG	ectopic expression of TbFlabarinL (pLEW100)
ZC130	Rv	GGAATCCGGCTCGAGTACTCGGATTTGTAICTCTGGAGACTATTCACC	ectopic expression of TbFlabarinL (pLEW100)
ZC139	Fw	CCGGAATCCCAAGCTTCCGCCACCATCGAGGTGCAACTTAACAGTTTAAACC	N-terminal tagging of PAR1 with 4xTY <i>in situ</i>
ZC140	Rv	CAACAATTCACAGACTACACAGTAACC	N-terminal tagging of PAR1 with 4xTY <i>in situ</i>
SH3	Fw	CCGGAATCCCAAGCTTATGGCTTGGAGCAATCCGCCGAAA	ectopic expression of TbFlabarin (pLEW100)
SH4	Rv	GGGAATCCCGGCTCGAGTACTCAAGTGGTCTTGGTTAGTATGACCTCGCGCGCCCTCGAACTCGGAAACCTTAA ACTTCGGAGCT	ectopic expression of TbFlabarin (pLEW100)
SH5	Fw	CCCGGAAATCCCAATTAATGAAGTGGGAAACTTAAGATTTGCCCGATG	C-terminal tagging of TbFlabarin with 4xTY <i>in situ</i>
SH6	Rv	GGGAATCCGGGATCCCGTCAACTCGGAAACACTTAACTTCGC	N-terminal tagging of TbFlabarinL with 4xTY <i>in situ</i>
SB13	Fw	ATGACCGAGTACAAGCCACG	binds in PAC ORF; integration PCR

Table 2.3. *Escherichia coli* strains

Strain	Genotype	Antibiotic resistance	Application	Prepared by
Top10 (Invitrogen)	F- mcrA Δ (mir-hsdRMS-mcrBC) Φ 80lacZ Δ M15 Δ lacX74 recA1 araD139 Δ (araleu)7697 galU galK rpsL (Str) endA1 nupG	Streptomycine	cloning/plasmid amplification	E.M. Natus
Roseta Blue (DE3) (Novagen)	F- ompT hsdSB(YB- mB-) gal dcm (DE3) pLysSRARE (CamR)	Chloramphenicol/Tetracycline	recombinant protein expression	E.M. Natus
JM110 (Stratagene)	rpsL (Str) thr leu thi-1 lacY galK galT ara tonA tsx dam dcm supE44 Δ (lac-proAB) [F' traD36 proAB lac t q Δ M15]	Streptomycine	cloning/plasmid amplification dam/dcm methylation free	J. Fraune

Table 2.4. *Trypanosoma brucei* cell lines

Cell line	Clone	Selection	Construct	Made by
2T1 TbFlabarinL ^{RNAi}	c5	2 µg/ml Phleomycin, 2 µg/ml Hygromycin	pRPAISL_TbFlabarinL RNAi	Z. Cicova
2T1 TbFlabarinL ^{RNAi}	c10	2 µg/ml Phleomycin, 2 µg/ml Hygromycin	pRPAISL_TbFlabarinL RNAi	Z. Cicova
2T1 TbFlabarinL ^{RNAi}	c12	2 µg/ml Phleomycin, 2 µg/ml Hygromycin	pRPAISL_TbFlabarinL RNAi	Z. Cicova
MITat1.2 SM Δ TbFlabarinL::PAC/ Δ TbFlabarinL::HYG	c2	2 µg/ml Neomycin, 1 µg/ml Puromycin, 2 µg/ml Hygromycin	PCR products: PAC and HYG ORF flanked by TbFlabarinL UTRs	Z. Cicova
MITat1.4 4xTY::TbFlabarinL/TbFlabarinL	c2	1 µg/ml Puromycin	p3077_PAC_4xTY_N-terminal tag_TbFlabarinL	Z. Cicova
AnTat1.1 Δ TbFlabarinL::PAC/ Δ TbFlabarinL::HYG	c2	1 µg/ml Puromycin, 2 µg/ml Hygromycin	PCR products: PAC and HYG ORF flanked by TbFlabarinL UTRs	Z. Cicova
MITat1.2 SM 4xTY::PAR1/PAR1	c3	2 µg/ml Phleomycin, 2 µg/ml Neomycin	p3077_PAC_4xTY_N-terminal tag_PAR1	Z. Cicova
29-13 BLE TbFlabarinL ^{Ti}	c1	15 µg/ml Neomycin, 2.5 µg/ml Hygromycin 2.5 µg/ml Phleomycin	pLEW100_BLE_TbFlabarinL	Z. Cicova
29-13 TbFlabarinL::4xTY/TbFlabarinL	c1	15 µg/ml Neomycin, 2.5 µg/ml Hygromycin 2.5 µg/ml Phleomycin	p3074_TbFlabarinL_4xTY_BLE	S. Hanselmann
MITat1.2 SM TbFlabarinL::4xTY/TbFlabarinL	c1	2 µg/ml Neomycin, 2 µg/ml Phleomycin	p3074_TbFlabarinL_4xTY_BLE	Z. Cicova
MITat1.2 SM TbFlabarinL ^{Ti}	c1	2 µg/ml Neomycin, 2 µg/ml Phleomycin	pLEW100_BLE_TbFlabarinL TY	S. Hanselmann

Table 2.5. Plasmids

Plasmid Name	Application	Construct	Resistance marker	Restriction enzyme (linearization prior to transfection into <i>T. brucei</i>)	Made by
pRPAiSL_TbFlabarinL RNAi	TbFlabarinL hairpin RNAi	TbFlabarinL (30-544 nt)	HYG	AscI	Z.Cicova
pETDUET1.1_TbFlabarinL	recombinant TbFlabarinL production in <i>E.coli</i>	10xHis tag_TbFlabarinL ORF	Amp	-	Z.Cicova
pLEW100v5b2x_TbFlabarinL	inducible ectopic expression of TbFlabarinL	TbFlabarinL ORF	BLE	NotI	Z.Cicova
pLEW100v5b2x_TbFlabarin	inducible ectopic expression of TbFlabarin with a C-terminal TY tag	TbFlabarin ORF_GlyAlaGly linker_TY tag	BLE	NotI	S. Hanselmann
p3077_PAC_4xTY_TbFlabarinL	N-terminal 4xTY tagging of TbFlabarinL <i>in situ</i>	4xTY_FlabarinL (0-607 nt)	Puro	HpaI	Z.Cicova
p3074_TbFlabarinL_4xTY_BLE	C-terminal 4xTY tagging of TbFlabarinL <i>in situ</i>	TbFlabarinL_4xTY (2-653 nt)	BLE	HpaI	Z.Cicova
p3074_TbFlabarin_4xTY_BLE	C-terminal 4xTY tagging of TbFlabarin <i>in situ</i>	TbFlabarin_4xTY (1-666 nt)	BLE	BclI	S.Hanselmann

Table 2.6. Antibodies

Antibody	Recognizes epitope	Primary (1)/secondary (2)	Dilution WB	Dilution IF	Animal	Polyclonal (P)/monoclonal (M)	Application	Reference
anti-TbFlabrinL	TbFlabrinL	1	1:500	1:200	rabbit	P	WB/IF	This study
L13D6	PFR	1	1:100	-	mouse	M	WB	68
TAT1	tubulin	1	1:2000	1:1000	mouse	M	WB/IF	69
BB2	TY	1	1:1000	1:500	mouse	M	WB/IF	70
anti-TbMORN1	MORN1	1	1:20 000	1:5000	rabbit	P	WB/IF	71
IRDye680	mouse IgG	2	1:20 000	-	donkey	P	WB	LI-COR Bioscience
IRDye800	rabbit IgG	2	1:20 000	-	donkey	P	WB	LI-COR Bioscience
Alexa 488	rabbit IgG	2	-	1:2000	goat	P	IF	Life Technologies/ Invitrogen
Alexa 594	mouse IgG	2	-	1:2000	goat	P	IF	Life Technologies/ Invitrogen

Table 2.7 Manual run Äktaprime

Action	Run Base (min)	Concentration of elution buffer (%)	Flow rate (ml/min)	Fraction size (ml)	Buffer valve position	Inject valve position
Priming (elution buffer)	2	100	40	0	1	waste
Priming (binding buffer)	2	0	40	0	1	waste
Equilibration	30	0	1	0	1	load
Autozero	-	-	-	-	1	-
Lysate application	50	0	0.1	0	1	inject
Wash 1	10	0	1	1	1	load
Wash 2	15	6	1	5	1	load
Elution	10	gradient elution from 0-100% elution buffer in 10 min	1	1	1	load
Wash with water	20	0	3	0	1	load
System wash with water	automatic	0	1	0	1	load
Wash with 20% ethanol	20 min	-	-	-	1	-
System wash with 20% ethanol	automatic	-	-	-	-	-
End	-	-	-	-	-	-

3 Results

3.1 *Tb*FlabarinL originated from a gene duplication event

*Tb*FlabarinL (Tb927.11.2400) was identified in a proteomic study⁵³ as a BSF specific, putative protein of unknown function. A BLAST search in the TriTryp database⁷⁰ found Tb927.11.2410, which is flagellar BAR domain protein homologue in *T. brucei*, *Tb*Flabarin. Alignment of *Tb*FlabarinL and *Tb*Flabarin using constraint-based multiple alignment tool (COBALT)⁷¹ revealed 38% amino acid identity and 60% similarity (Fig. 3.1).

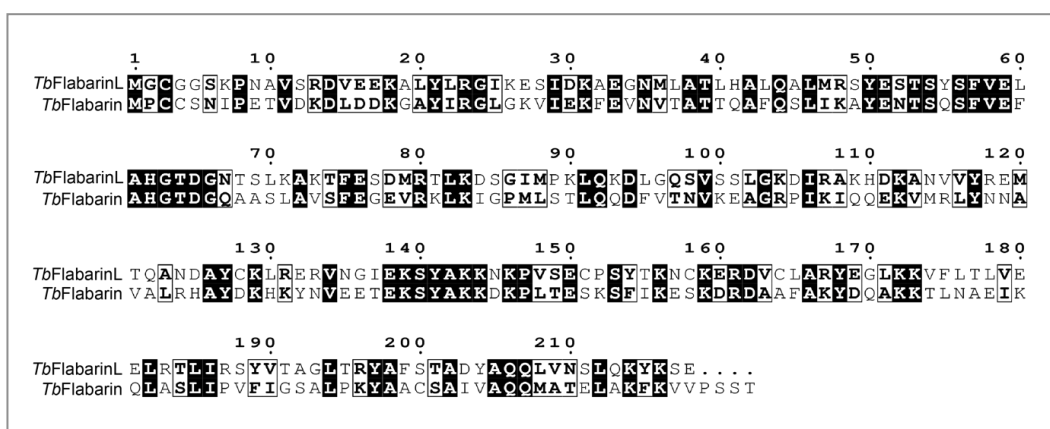


Figure 3.1. Alignment of *Tb*FlabarinL (Tb927.11.2400) to *Tb*Flabarin (Tb927.11.2410).

BLAST search against *Tb*FlabarinL protein sequence found *Trypanosoma brucei* flabarin homologue Tb927.11.2410. Amino acid sequences of *Tb*FlabarinL and *Tb*Flabarin were aligned using constraint-based multiple alignment tool (COBALT)⁷¹. They share 38% amino acid identity (indicated by black boxes) and 60% similarity (indicated by white boxes).

*Tb*Flabarin consists almost entirely of a BAR/IMD like domain, which extends over the region of 8-212 amino acids (AA) out of a total 222 AA length of the protein. Despite the 60% similarity to *Tb*Flabarin (Fig. 3.1), a BAR/IMD like domain is missed by the prediction software in *Tb*FlabarinL. However, structural models predicted by protein homology/analogy recognition engine V2.0 (Phyre2) server⁷³ of both *Tb*Flabarin and *Tb*FlabarinL feature a triple helix coiled coil architecture (Fig. 3.2). Such a structure is characteristic of BAR proteins and enables formation of banana shaped homo- or heterodimers well known for their membrane curvature generation (reviewed in⁹³).



Figure 3.2. Structure models of *TbFlabarinL* and *TbFlabarin*.

Structure model of *TbFlabarinL* (A) and *TbFlabarin* (B) predicted by protein homology/analogy recognition engine V2.0 (Phyre2) server⁷³. (C) Overlay of *TbFlabarinL* and *TbFlabarin* structure models.

TbFlabarin and *TbFlabarinL* are both found on chromosome 11 separated by a ~12 kb stretch of a non-coding sequence. The *TbFlabarin* coding sequence (CDS) is on the complementary DNA strand. Each gene is a part of different polycistronic transcription unit (PTU) that face each other in the opposite directions⁹⁴ (Fig. 3.3). *TbFlabarinL* and *TbFlabarin* are the last genes of their respective PTUs.



Figure 3.3. Arrangement of *TbFlabarinL* and *TbFlabarin* on chromosome 11

TbFlabarinL and *TbFlabarin* are the ends of two different polycistronic transcription units (PTUs) separated by 12 kb stretch of non-coding DNA. Each PTU is transcribed from the opposite direction.

Orthologs of *TbFlabarinL* are present within the orthology group OG5_185161 from Ortho MCL DB^{95,96} in *T. brucei gambiense*, *T. vivax* and *T. evansi*. In contrast to *TbFlabarin* (OG5_148786), *TbFlabarinL* is not present in the sequenced evolutionary older Kinetoplastea (Fig. 3.4). A phylogenetic analysis revealed a gene duplication event only in African trypanosomes that gave rise to the FlabarinL gene (Fig. 3.4). Interestingly, FlabarinL gene is present in *T. vivax* and missing in *T. congolense* and *T. equiperdum*.

Why has *T. brucei* two paralogs of such an identity? In order to unravel possible different functions of these paralogs, we first searched for information about potential stage specific regulation of these proteins. Indeed, the results of a differentiation proteome⁹⁷, in which pleomorphic trypanosomes were differentiated from BSF to PCF show that *TbFlabarinL* is

downregulated 24 hours post induction of differentiation and undetectable in PCF. In contrast, *TbFlabarin* is upregulated very early during differentiation process (2 hours after induction) and is fully expressed 24 hours post induction⁹⁷. Protein expression levels of *TbFlabarinL* are 20-fold higher in BSF compared to PCF⁵³, which suggests that this protein might be a potential mammalian host specific adaptation factor and an obvious target for a genetic intervention for a detailed analysis.

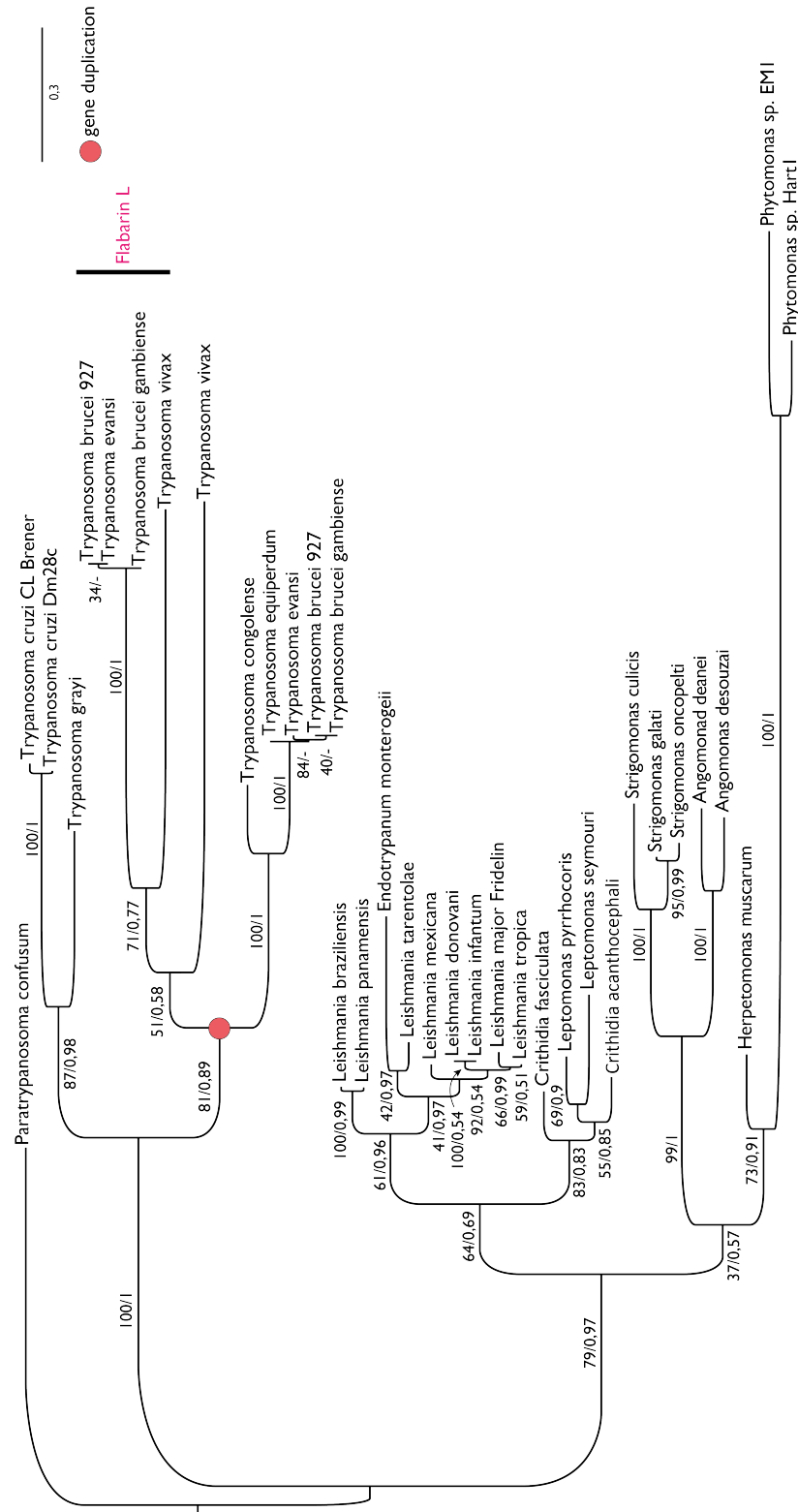


Figure 3.4. Phylogenetic analysis of Flabarins across Trypanosomatida.*

A maximum likelihood phylogenetic tree based on alignments of Flabarin and FlabarinL proteins. The scale bar indicates the inferred number of amino acid substitutions per site. The red dot indicates a gene duplication event that gave rise to the FlabarinL gene, which is present only in certain species of the African trypanosomes.

*These data were generated with support from Tomas Skalicky.

To confirm the expression profiles of the mass spectrometry study, we generated a *TbFlabarinL* specific antibody. The ORF of *TbFlabarinL* fused to a 10x His-tag with a Gly-Ala-Gly linker at the N-terminus was cloned into pETDUET-1 expression vector. Recombinant *TbFlabarinL* was expressed in 800 ml of Rosetta Blue *E. coli* culture upon induction with 1 mM IPTG for 3 h at 37°C. Recombinant *TbFlabarinL* was purified using Äkta prime fast liquid protein chromatography (FPLC) and a HisTrap FF Crude column. Samples from every other purification fraction were separated by SDS-PAGE and stained with Coomassie brilliant blue (Fig 3.5). Fractions containing recombinant *TbFlabarinL* (9-23) were pooled, dialyzed and concentrated using a centrifugal unit with a 10 kDa cut off. Two contaminant bands migrating around 15 kDa were co-purified in the fractions containing recombinant *TbFlabarinL* (Fig. 3.5). The amount of the contaminant proteins was very low compared to the amount of recombinant *TbFlabarinL*. The protein concentration determined by Bradford assay was 6.6 mg/ml. 500 µg of recombinant *TbFlabarinL* was used for immunization of a rabbit.

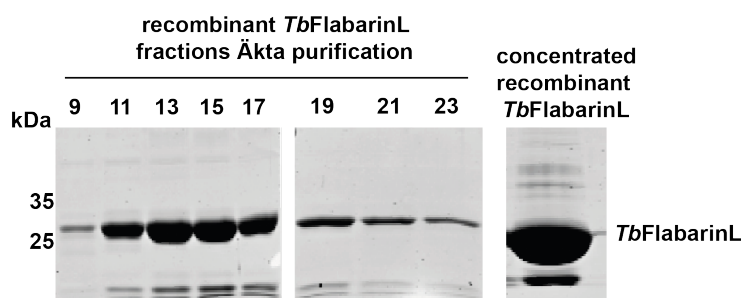


Figure 3.5. Purification of recombinant *TbFlabarinL*.

Recombinant *TbFlabarinL* fused to a 10x His-tag with a Gly-Ala-Gly linker at the N-terminus was expressed and purified from *E. coli* using an Äkta FPLC and a HisTrap FF crude column. Fractions containing recombinant *TbFlabarinL* (9-23) were pooled, dialyzed and concentrated using a centrifugal filter unit with a 10 kDa cut off. Every other fraction containing the purified *TbFlabarinL* and a sample of the concentrated recombinant *TbFlabarinL* were separated by SDS-PAGE and stained with Coomassie brilliant blue.

TbFlabarinL specific antibody was affinity purified from the immune sera and used in WB analysis (Fig. 3.6). A band of the expected molecular weight could be detected in BSF whole cell lysates but not in lysates from PCF confirming that *TbFlabarinL* is a stage specific protein. Recombinant *TbFlabarinL* was used as a positive control. Besides the expected band migrating at 25 kDa, another band of 55 kDa was detected. Five cysteines are

present within *TbFlabarinL*. Disulfide bridges could be built upon oxidation of the cysteine thiol group and lead to formation of homodimers of *TbFlabarinL* that migrate at 55 kDa.

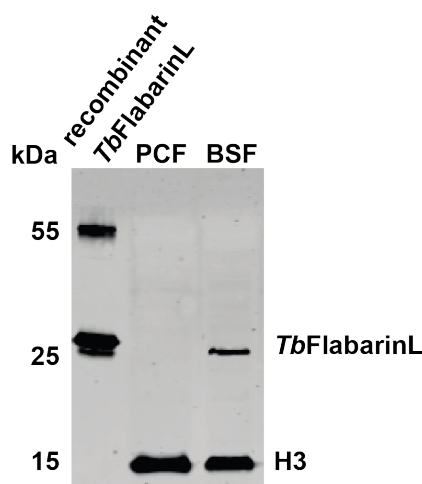


Figure 3.6. *TbFlabarinL* is a BSF stage-specific protein.

WB analysis using affinity purified *TbFlabarinL* specific antibody confirms the 20-fold upregulation of *TbFlabarinL* in BSF compared to PCF. Immunoblotting with anti-Histone H3 served as a loading control of whole cell lysates.

3.2 *TbFlabarinL* is not an essential gene

In order to examine the effect of *TbFlabarinL* depletion on the viability of *T. brucei*, an inducible RNAi knock down cell line was generated. Sense and antisense fragments of the RNAi hairpin were cloned into pRPAiSL single locus targeting vector⁹⁸ and linearized construct was transfected into 2T1 cells. RNAi was induced by addition of 1 μ g/ml tetracycline to the cell culture. Whole cell lysates of parental 2T1 cell line, Tet- and 24, 48, 72 or 96 h after induction of RNAi (Tet+) were separated by SDS-PAGE. WB analysis using *TbFlabarinL* specific antibody revealed significant reduction of *TbFlabarinL* expression 24 h after induction of RNAi (Fig. 3.7A). *TbFlabarinL* levels were below detection 48 h after induction of RNAi (Fig. 3.7A). The growth of the parasites upon induction of RNAi was monitored (Fig. 3.7B). There was no growth phenotype observed upon depletion of *TbFlabarinL* (Fig. 3.7), indicating that *TbFlabarinL* is not an essential gene for the survival of the parasite under cell culture conditions.

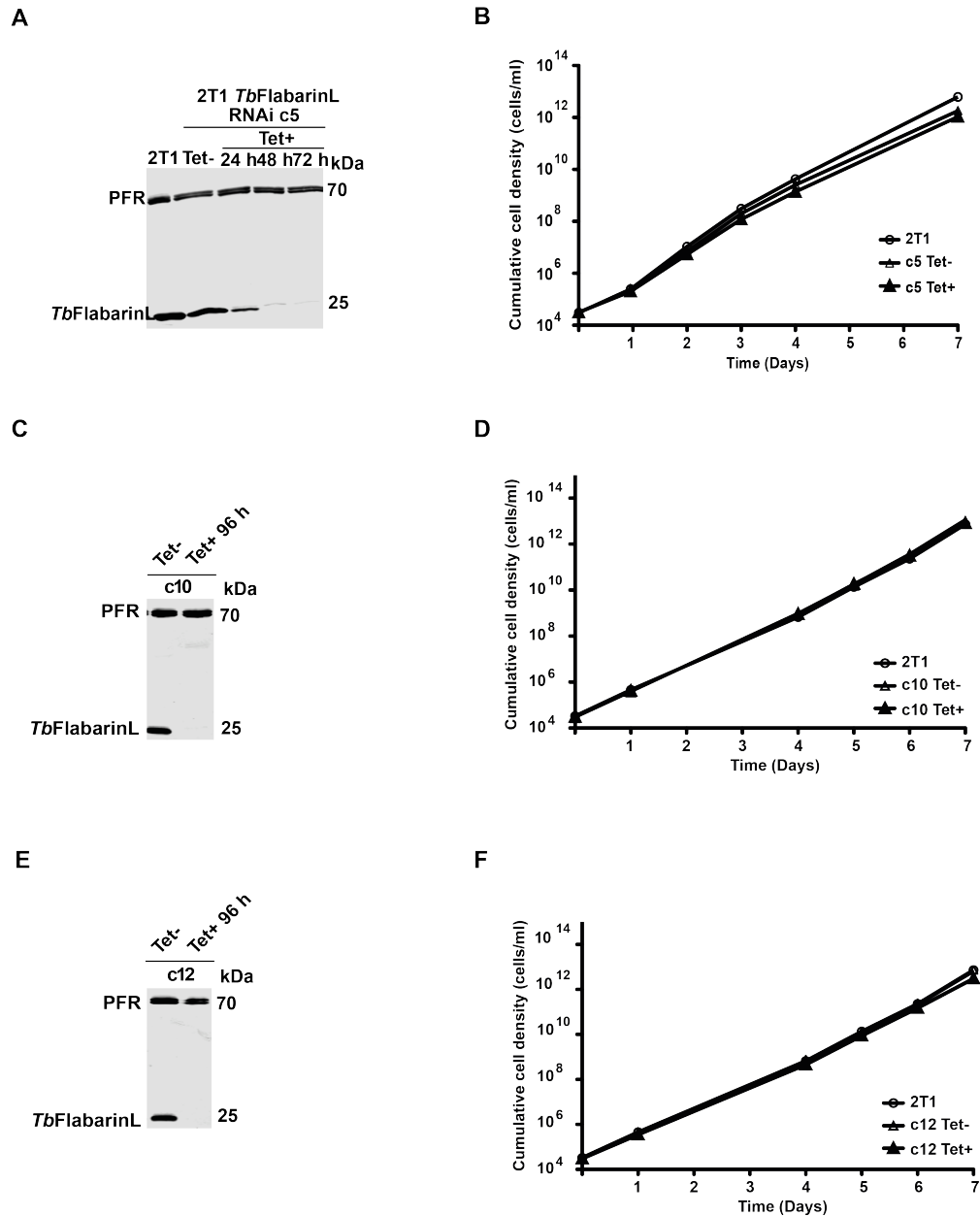


Fig 3.7. *TbFlabarinL* RNAi in BSF *T. brucei*.

(A) *TbFlabarinL* protein is reduced below the level of detection 48 h after induction of RNAi as determined by *TbFlabarinL* specific antibody immunoblot. Immunoblot with anti-PFR antibodies was used as a loading control. **(B)** Depletion of *TbFlabarinL* by RNAi has no effect on the growth of *T. brucei* under cell culture conditions. Parental 2T1 cell line and Tet- cells were used as controls. WB and growth curve (n=1) of one representative clone. **(C) (D) (E) (F)** WB and growth curve after depletion of *TbFlabarinL* in two additional clones.

To further pursue the indication that *TbFlabarinL* is not essential for the survival of the parasite under cell culture conditions, knock out cell line ($\Delta TbFlabarinL$) was generated in BSF trypanosomes by homologous recombination. First, one allele of *TbFlabarinL* was replaced by puromycin N-acetyl-transferase ORF resulting in the single knock out *TbFlabarin* +/- cell line. In the second step, the second allele of *TbFlabarin* was replaced by hygromycin phosphotransferase ORF in the *TbFlabarin* +/- cell line resulting in deletion of both alleles. The deletion of both *TbFlabarinL* alleles was verified by integration PCR (Fig. 3.8A). Primers binding in the 5' and 3'UTRs, in the ORF of *TbFlabarinL* and in the hygromycin and puromycin resistance ORFs were used (Fig 3.8B). The parental cell line (WT) and the *TbFlabarinL* +/- cell lines were used as controls. In the first three lanes a pair of primers binding in the 5' and 3'UTR outside of the recombination sites was used. In the first lane, a band of the expected size 924 bp corresponding to the WT alleles was detected in the WT cells. In the second lane, a band of puromycin resistance ORF of 814 bp and a band of 924 bp were detected as expected in the *TbFlabarin* +/- cell line. In the third lane a band of 1296 bp corresponding to the hygromycine resistance ORF and a band of 814 bp of the puromycin resistance ORF were detected as expected in the $\Delta TbFlabarinL$ cell line. In the lanes four to six, primers binding at the 5' and 3'end of the *TbFlabarinL* ORF were used. In the fourth and the fifth lane a band of 654 bp was detected, which corresponds to the *TbFlabarinL* ORF and was expected in the WT and the *TbFlabarin* +/- cell line. No amplificate was detected in the sixth lane as expected in the $\Delta TbFlabarinL$ cell line, where both alleles of *TbFlabarinL* were deleted. Primer pair binding in the hygromycine resistance ORF and 3'UTR was used in the lanes seven to nine. No band was detected in the lane seven and eight in the WT and *TbFlabarin* +/- cell lines. A band of 858 bp was detected in the lane nine, which corresponds to the hygromycin resistance ORF fragment and was expected in the $\Delta TbFlabarinL$ cell line. Primers binding in the puromycin resistance ORF and 3'UTR were used in the lanes ten to twelve. No band was detected in the lane ten as expected in the WT cells. A band of 674 bp, which corresponds to the puromycin resistance ORF fragment, was detected in the lanes eleven and twelve as expected in the *TbFlabarinL* +/- and $\Delta TbFlabarinL$ cell lines. WB analysis of whole cell lysates from a pool (non-clonal population) and two clones c1 and c2 using the *TbFlabarinL* specific antibody further verified the deletion of both *TbFlabarinL* alleles. WT BSF and PCF whole cell lysates were used as a control. A very faint unspecific

band migrating slightly higher than *TbFlabarinL* was detected in the $\Delta TbFlabarinL$ cell line (Fig. 3.8C). Growth of the WT and one representative clone of the $\Delta TbFlabarinL$ cell lines was monitored and no difference was observed (Fig. 3.8D), which confirms that *TbFlabarinL* is not an essential gene for the survival of *T. brucei* under cell culture conditions.

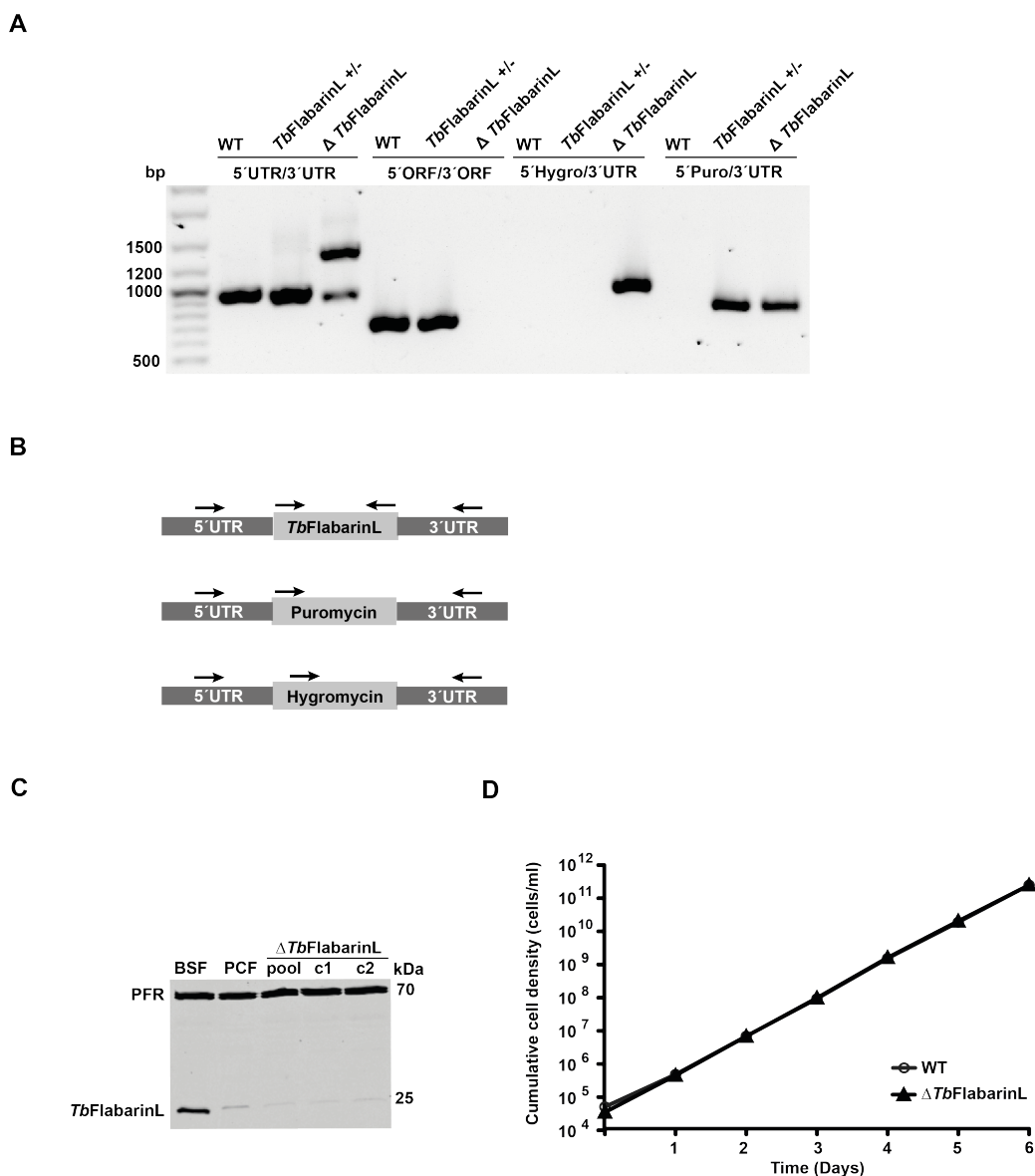


Figure 3.8. *TbFlabarinL* deletion in the monomorphic BSF *T. brucei*.

(A) Integration PCR verified the correct integration of puromycin N-acetyl-transferase and hygromycin phosphotransferase ORFs that replaced both alleles of *TbFlabarinL* gene. **(B)** Primers binding in the 5' and 3'UTR, 5' and 3'ORF and within the puromycin and hygromycin resistance ORFs were used. **(C)** WB analysis using *TbFlabarinL* specific antibody confirmed deletion of *TbFlabarinL*. Immunoblot with anti-PFR antibodies was used as a loading control. **(D)** There was no difference in the growth of $\Delta TbFlabarinL$ representative clone and the parental cell line (WT); (n=3).

3.3 *TbFlabarinL* is dispensable for developmental differentiation

TbFlabarinL has a very interesting expression profile during developmental differentiation. It is highly upregulated in LS and SS forms, still detectable during early differentiation but is downregulated below detection levels 48h after induction of differentiation⁹⁷. To test the hypothesis, that *TbFlabarinL* could be involved in BSF to PCF transition, a stable $\Delta TbFlabarinL$ cell line was generated in a pleomorphic *T. brucei* strain. So-called monomorphic parasites, which we used in the previous experiments, are culture adapted and very convenient for reverse genetics, but initiation of differentiation is inherently inefficient and asynchronous. In pleomorphic strains of *T. brucei*, differentiation is very efficient and both steps of the differentiation process (LS to SS and SS to PCF) can be monitored in cell culture. Furthermore, pleomorphic strains still respond to stumpy-inducing factor (SIF) with growth arrest *in vivo* and are therefore the better system to study differentiation cell biology and virulence *in vivo*. Hence, we generated pleomorphic $\Delta TbFlabarinL$ trypanosomes (in strain AnTat1.1) as described above. The loss of both *TbFlabarinL* alleles was verified by integration PCR (Fig. 3.9A) using primer combinations as shown in Fig. 3.9B. The parental AnTat1.1 cell line was used as a control. A band of 924 bp, which corresponds to *TbFlabarinL* fragment expected in the WT cell line, was amplified in the lane one using primers binding in the 5' and 3'UTRs. As expected in the WT cell line, no specific bands were amplified in the lanes two and three, where primer pair binding in the hygromycin resistance ORF and 3'UTR and puromycin resistance ORF and 3'UTR were used. A band of 654 bp, which corresponds to the *TbFlabarinL* ORF as expected in the WT cell line, was amplified using primers binding at the 5' and 3' end of the *TbFlabarinL* ORF in the lane four. Two bands 1296 bp and 814 bp, which correspond to the hygromycine resistance ORF and puromycin resistance ORF, were amplified in the lane five using primers binding in the 5' and 3'UTRs as expected in the $\Delta TbFlabarinL$ cell line. A band of 445 bp, which corresponds to the hygromycine resistance ORF fragment, was detected in the lane six as expected in the $\Delta TbFlabarinL$ cell line. A band of 674 bp, which corresponds to the puromycin resistance ORF fragment, was detected in the lane seven as expected in the $\Delta TbFlabarinL$ cell line. No specific band was detected in the lane eight, where primers binding at the 5' and 3' end of the *TbFlabarinL* ORF were used. This was expected in the $\Delta TbFlabarinL$ cell line. The deletion of *TbFlabarinL* ORF was further confirmed in WB analysis (Fig. 3.9C). Next, the growth of the $\Delta TbFlabarinL$ cell line was compared to the parental cell line

and no pronounced growth phenotype was observed (Fig. 3.9D), which is concordance with the result seen in the monomorphic $\Delta TbFlabarinL$ cell line (Fig 3.8D). In the next step, the pleomorphic cells were grown to a high density to induce SS formation and then further differentiated for 52 hrs. $\Delta TbFlabarinL$ and parental cells grew equally well during developmental differentiation (Fig. 3.9F), which suggests that *TbFlabarinL* is dispensable for this process. WB analysis (Fig. 3.9E) of whole cell lysates of WT LS, SS, and cells 2, 28 and 56 h after induction of differentiation confirmed the downregulation of *TbFlabarinL* during differentiation seen in proteomic analysis⁹⁷. Whole cell lysates of $\Delta TbFlabarinL$ SS and cells 52 h after induction of differentiation were loaded as a control. A second very faint band migrating slightly higher than *TbFlabarinL* was detected by anti-*TbFlabarinL* antibody in the $\Delta TbFlabarinL$ cell lines after induction of differentiation. This band is detectable in the WT pleomorphic cells during differentiation from SS to PCF at the time point of 28 h post differentiation, when the *TbFlabarinL* band becomes weaker. The same band is detectable during the differentiation of $\Delta TbFlabarinL$ at the time point 52 hours. To exclude that *TbFlabarinL* specific antibody can recognize *TbFlabarin*, WB analysis of a BSF cell line ectopically expressing TY epitope tagged *TbFlabarin* was performed (Fig. 3.10). Both *TbFlabarinL* specific and anti-TY antibodies could only detect one band, which supports the quality of the *TbFlabarinL* specific antibody. Whole cell lysate from cells without addition of Tet was used as a control.

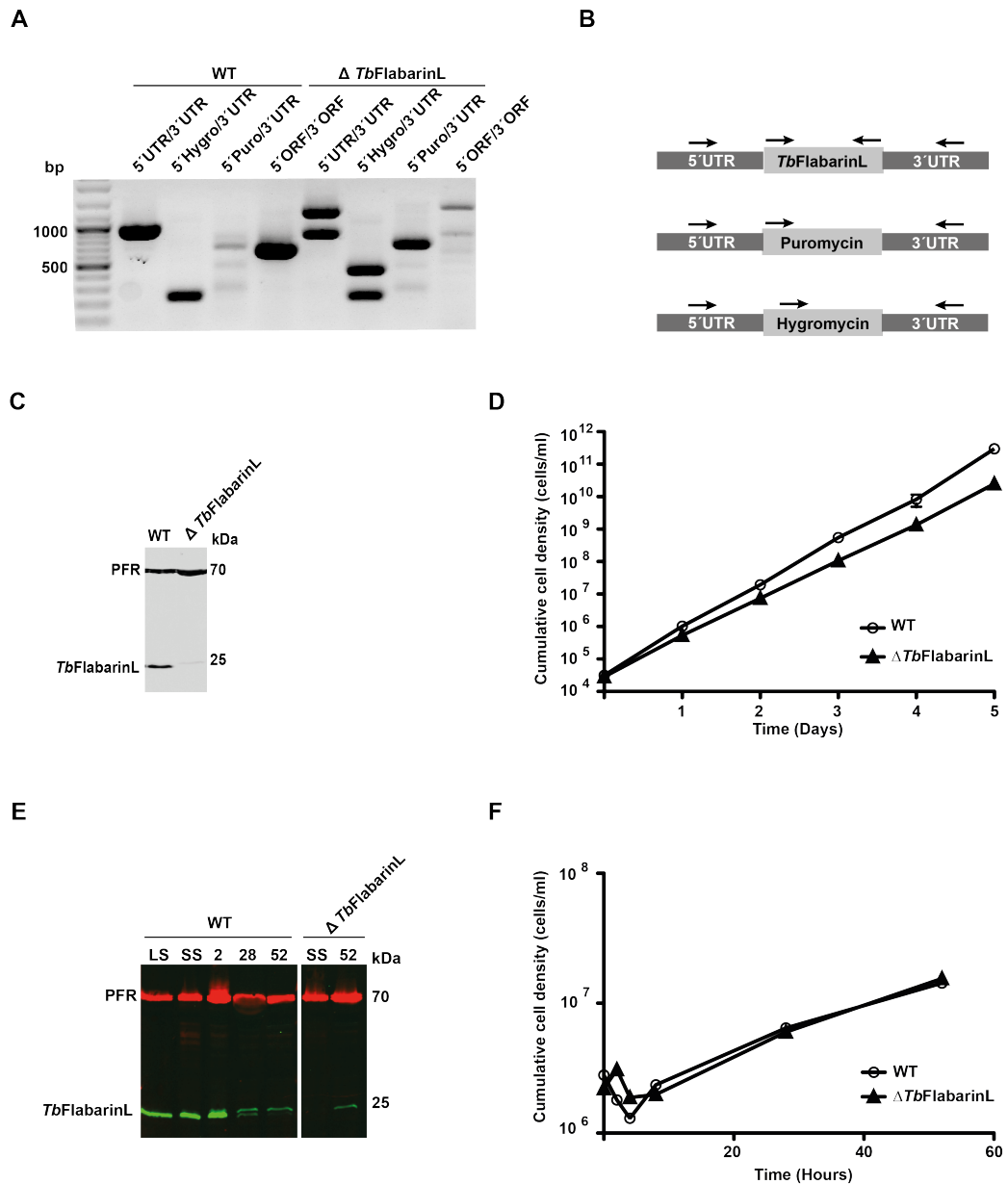


Figure 3.9. *TbFlabarinL* deletion in the pleomorphic BSF *T. brucei*.

(A) Integration PCR verifies the correct integration of puromycin N-acetyl-transferase and hygromycin phosphotransferase ORFs that replaced both alleles of *TbFlabarinL* gene. **(B)** Primers binding in the 5' and 3'UTR, 5' and 3'ORF and within the puromycin and hygromycin resistance ORFs were used. **(C)** WB analysis using *TbFlabarinL* specific antibody confirmed deletion of *TbFlabarinL*. Immunoblot with anti-PFR antibodies was used as a loading control. **(D)** There was no pronounced difference in the growth of Δ *TbFlabarinL* representative clone and the parental cell line (WT); (n=3). **(E)** WB analysis using *TbFlabarinL* specific antibody confirmed downregulation of *TbFlabarinL* during differentiation. Immunoblot with anti-PFR antibodies was used as a loading control. **(F)** Pleomorphic trypanosomes were successfully differentiated from LS to PCF. There was no difference in the growth rate between the parental (WT) and Δ *TbFlabarinL* cell line; (n=1).

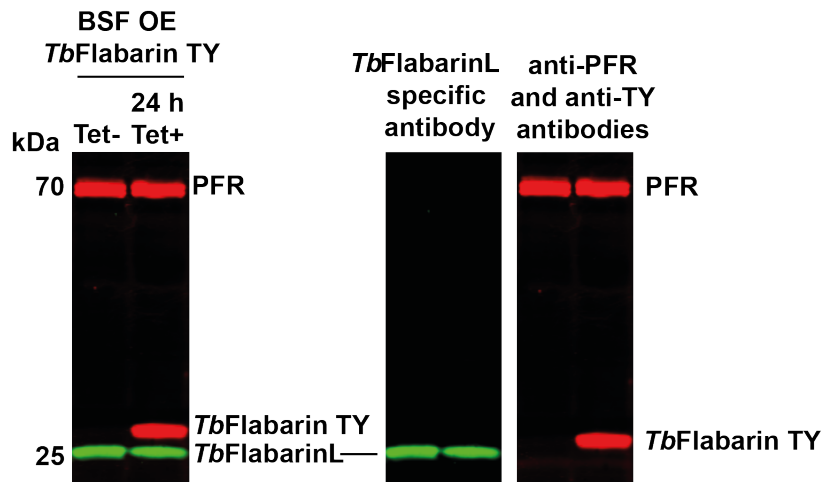


Figure 3.10. Anti-*TbFlabarinL* antibody recognizes *TbFlabarinL* but not *TbFlabarin*

WB analysis of whole cell lysates of a cell line that expresses Ty tagged *TbFlabarin* after Tet induction using *TbFlabarinL* specific antibody (green) and anti-TY (red) antibodies shows that *TbFlabarinL* specific antibody recognizes only *TbFlabarinL*. Immunoblot with anti-PFR antibodies (red) was used as a loading control. The *TbFlabarinL* specific antibody does not cross-react with the *TbFlabarin* even though the two proteins share 38% identity at the amino acid level.

Further confirmation that the unspecific band detected in the Δ *TbFlabarinL* is not *TbFlabarin* was provided by label free mass spectrometry comparison of WT and Δ *TbFlabarinL* cells (Fig. 3.11). Four biological replicates of each cell line were lysed and subjected to mass spectrometry analysis. As expected *TbFlabarinL* was enriched in the WT compared to the Δ *TbFlabarinL* cells. *TbFlabarin* was not detected among the proteins enriched in the Δ *TbFlabarinL* cell line.

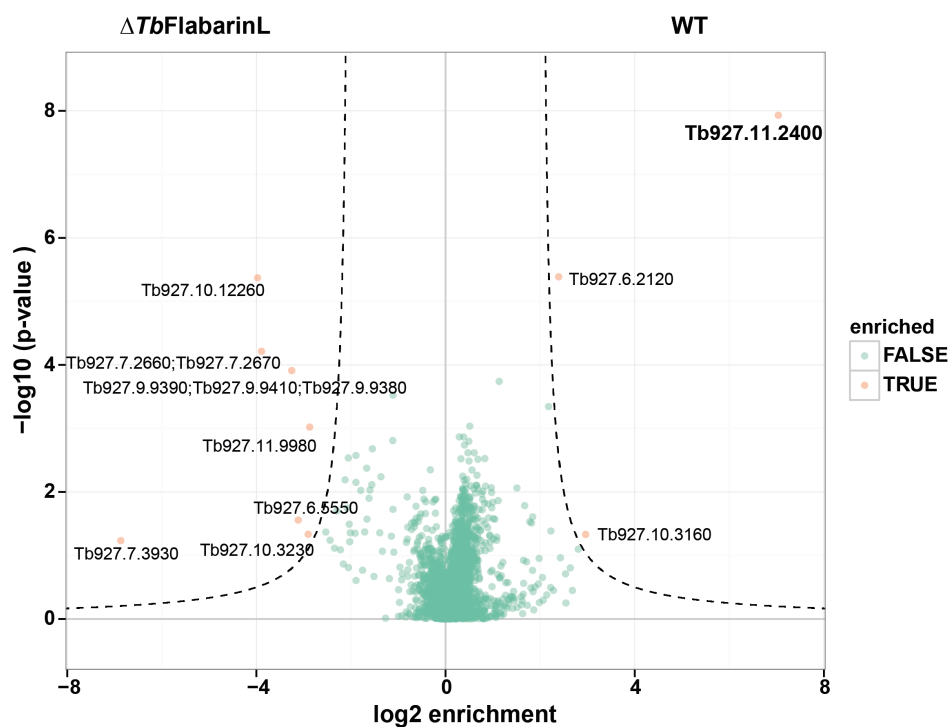


Figure 3.11. Label free mass spectrometry comparison of WT and $\Delta TbFlabarinL$ cell lines**

Four biological replicates of WT and $\Delta TbFlabarinL$ cells were lysed and subjected to mass spectrometry analysis. *TbFlabarinL* was enriched in the WT cells. *TbFlabarin* was not among the proteins detected in the $\Delta TbFlabarinL$ cells.

**Falk Butter performed the mass spectrometry and statistical analyses.

In summary, *TbFlabarinL* is not essential for growth and differentiation of *T. brucei* under cell culture conditions. We could not observe any significant differences between WT trypanosomes and *TbFlabarinL*-depleted parasites during the course of infection in mice⁹⁹. Since deletion of *TbFlabarinL* did not reveal any hint for a possible function of *TbFlabarinL*, the focus was shifted to the potential interacting partners of *TbFlabarinL*.

3.4 *TbFlabarinL* is associated with the paraflagellar rod and the flagellar membrane

In order to find interacting partners of *TbFlabarinL*, *TbFlabarinL* specific antibody was used in a co-immunoprecipitation experiment. *TbFlabarinL* specific antibody was immobilized to protein G sepharose beads and non-specific binding was blocked with BSA. Four biological replicates of WT and $\Delta TbFlabarinL$ cell line were lysed and incubated with the beads. After

washing steps, the proteins bound to the beads were eluted. The eluates were analyzed by mass spectrometry. Two interacting partners Tb927.11.3840 and Tb927.11.13500 (Fig. 3.12A) were found. The first interacting partner is a putative protein with no conserved domains that could shed some light on the function of this candidate. The second interacting partner is PAR1, a previously described paraflagellar rod component¹⁰⁰⁻¹⁰². To verify the result of the co-immunoprecipitation, the PAR1 ORF was fused to a sequence that encodes for a 4xTY epitope tag by homologous recombination. These cells were stained with anti-TY antibody for immunolocalization studies. As expected, TY-PAR1 localized to the flagellum (Fig. 3.10B). Detection with anti-TY and anti-*TbFlabarinL* antibodies showed an overlap of *TbFlabarinL* and 4xTY::PAR1 in distinct parts of the flagellum, which corroborated the result of the co-immunoprecipitation.

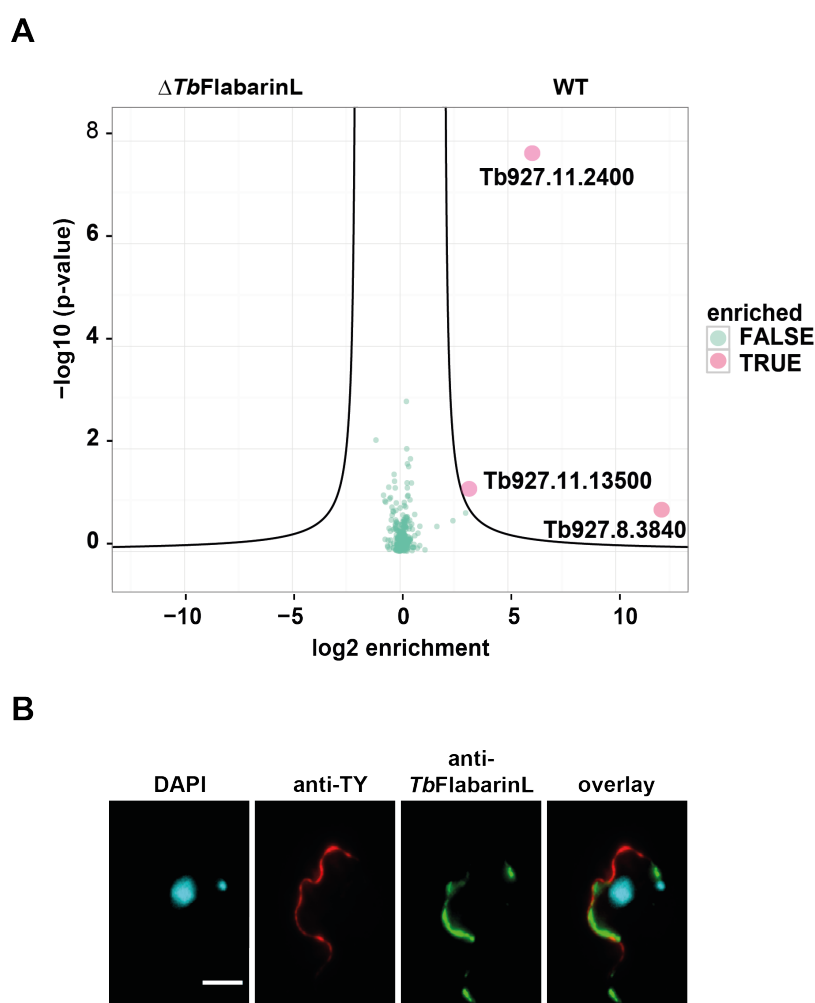


Figure 3.12. Co-immunoprecipitation using *TbFlabarinL* specific antibody.**

(A) Volcano plot of the interaction data for *TbFlabarinL* obtained by label-free quantitative mass spectrometry of four biological replicates of WT and control $\Delta TbFlabarinL$ cell lines. Besides the bait protein, two more proteins were enriched: Tb927.11.3840 and Tb927.11.13500. The first interacting partner is an unknown putative protein. The second interacting partner is PAR1, a paraflagellar rod component. **(B)** *In situ* N-terminally TY-tagged PAR1 localizes to the flagellum (red). Immunofluorescence analysis using the *TbFlabarinL* specific antibody (green) shows that *TbFlabarinL* localizes to the flagellum of *T. brucei*. A co-staining of anti-TY (red) and *TbFlabarinL* specific (green) antibody shows *TbFlabarinL* and PAR1 overlap in certain regions of the flagellum. DNA stained with DAPI (cyan). Scale bar 3 μm .

**Falk Butter performed the mass spectrometry and statistical analyses.

Interestingly, *TbFlabarinL* localization revealed a different pattern compared to PAR1. Immunofluorescence staining using *TbFlabarinL* specific antibody showed an interrupted pattern throughout the flagellum (Fig. 3.12B and Fig. 3.13). Staining with TAT1 anti-tubulin antibody was used to visualize the cell body and flagellum. PCF and Δ *TbFlabarinL* cells were used as a control.

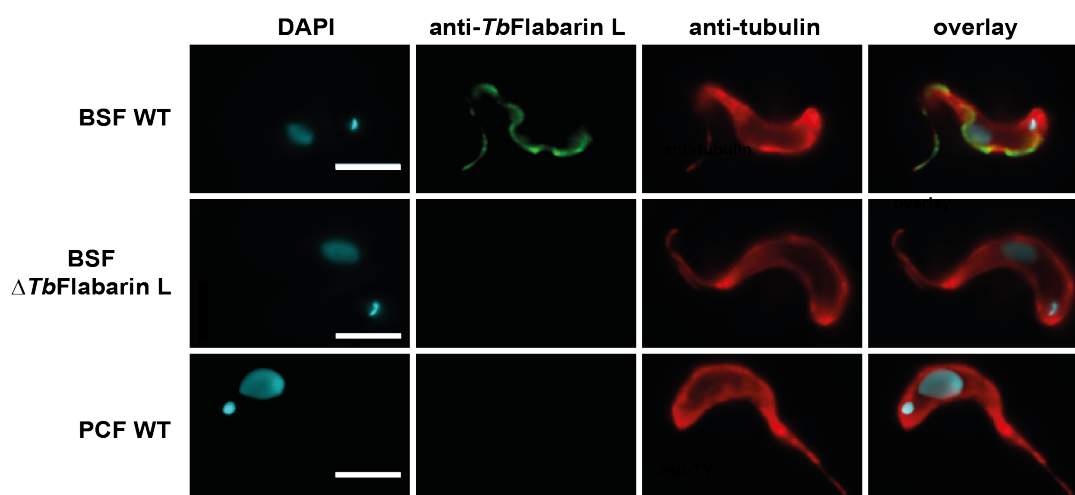


Figure 3.13. *TbFlabarinL* is localized to the flagellum.

Immunofluorescence analysis using the *TbFlabarinL* specific antibody (green) shows that *TbFlabarinL* localizes to the flagellum of *T. brucei*. Staining with TAT1 anti-tubulin antibody (red) was used to visualize the cell body and flagellum. The *TbFlabarinL* depleted cell line and PCF served as negative controls. DNA stained with DAPI (cyan). Scale bar 3 μ m.

In a previous experiment we observed that N-terminal tagging of *TbFlabarinL* resulted in a mislocalization of *TbFlabarinL*. The cells where the ORF of only one allele was fused to a sequence that encodes for a 4xTY epitope tag by homologous recombination were stained with anti-TY and *TbFlabarinL* specific antibodies. The tagged version of *TbFlabarinL* remained in the cytoplasm (Fig. 3.14A). Interestingly, the first 24 N-terminal AAs of *TbFlabarinL* share 75% identity with the N-terminal sequence of flagellar calcium binding protein (FCaBP) in *T. cruzi* (Fig. 3.14B). The first 24 AAs, the presence of a myristoylated glycine in position 2 and palmitoylated cysteine in position 4 and the conserved and positively charged lysines, are responsible for flagellar localization and for the association of FCaBP with the inner leaflet of the flagellar membrane⁶⁶. *TbFlabarinL* contains glycine in position 2 and cysteine in position 3 and two positively charged lysines. The similarity of the N-termini of *TbFlabarinL* and FCaBP and mislocalization of *TbFlabarinL* after *in-situ* N-terminal tagging implies that *TbFlabarinL*

flagellar membrane association is mediated by similar targeting mechanisms.

Figure 3.14. *In situ* N-terminal tagging results in mislocalization of *TbFlabarinL* to the cytoplasm.

(A) The N-terminally Ty-tagged *TbFlabarinL* (red) shows a spotty localization pattern within the cytosol whereas the *TbFlabarinL* WT protein (green) localizes to the flagellum. *TbFlabarinL* specific antibody recognizes both the WT and the tagged allele of *TbFlabarinL*. Thus, the green signal in the cytoplasm detected by the anti-TY antibody corresponds to the tagged allele of *TbFlabarinL*. DNA stained with DAPI (cyan). Scale bar 3 μ m. **(B)** The N-terminus of *TbFlabarinL* is similar to N-terminal sequences of Flagellar Calcium Binding Protein (FCaBP) of *T. cruzi*. Elements potentially necessary for the association with the flagellar membrane are highlighted. Palmitoylated and myristoylated amino acids are marked in red and blue, respectively. Conserved lysines are marked in yellow.

To further analyze the similarity of *TbFlabarinL* and *TbFlabarin* and to test if similar targeting mechanisms apply for the procyclic protein, C-terminally TY epitope tagged *TbFlabarin* was expressed in the BSF (Fig. 3.15A). *TbFlabarin* localized clearly to the flagellum with a discontinuous pattern similar to that of *TbFlabarinL* (Fig. 3.15A). Staining with anti-TY and *TbFlabarinL* specific antibodies shows an overlap of the signal in distinct regions of the flagellum (Fig. 3.15A). Reversely, ectopically overexpressed *TbFlabarinL* in PCF localized to the flagellum in a more continuous pattern along the whole length of the flagellum (Fig. 3.15B) presumably due to high expression levels (200-fold overexpression compared to endogenous protein levels in PCF). *In situ* C-terminally TY-tagged *TbFlabarin* in PCF localized to the flagellum and displayed a patchy pattern similar to that of *TbFlabarinL* in BSF (Fig. 3.15C).

These observations are in line with the hypothesis that *TbFlabarinL* and *TbFlabarin* have a similar stage-specific function in the flagellum of *T. brucei*.

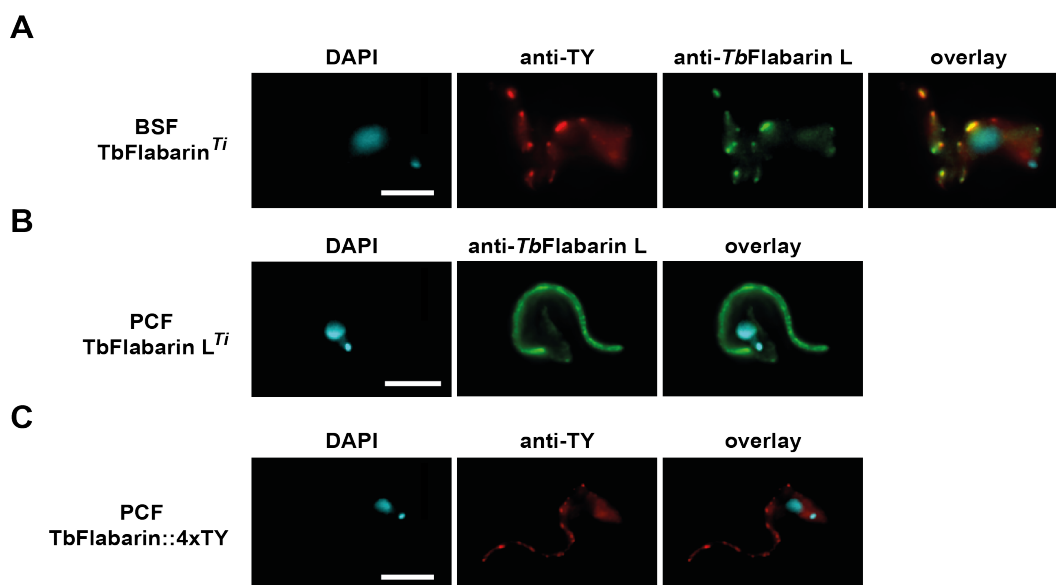


Figure 3.15. *TbFlabarin* and *TbFlabarinL* localization in the BSF and PCF *T. brucei*.

(A) Immunofluorescence staining using anti-TY (red) and *TbFlabarinL* specific (green) antibodies depicts that ectopically expressed *TbFlabarin* in BSF has a similar patchy localization pattern as *TbFlabarinL* and that the localization of the two proteins overlaps in some regions. **(B)** Ectopically expressed *TbFlabarinL* localizes in the flagellum in PCF as shown by immunofluorescence staining using *TbFlabarinL* specific antibody. **(C)** Immunofluorescence staining using anti-TY antibody to visualize *in situ* C-terminally TY tagged *TbFlabarin* in PCF shows a similar pattern to the localization of *TbFlabarinL* in BSF in the flagellum. DNA stained with DAPI (cyan). Scale bar 3 μm.

The results of the co-immunoprecipitation experiment as well as the partial overlap of PAR1 and *TbFlabarinL* immunostaining imply association of *TbFlabarinL* with the PFR structure of the flagellum. In contrast, the N-terminal sequence of *TbFlabarinL* seems to attach *TbFlabarinL* to the flagellar membrane. To unravel the exact membrane association of *TbFlabarinL*, a biochemical cell fractionation was performed (Fig. 3.16A). In the first step, the detergent soluble fraction S1 (cytoplasm/membranes) was separated from P1 (cytoskeleton). In the second step, the cytoskeletal fraction P1 was treated with 1 M KCl to depolymerize the microtubule corset and FAZ and thus separate S2 (corset microtubules together with FAZ) from P2 (PFR, axoneme, basal body and flagellar collar). WB analysis of equal fractions (10% of input material) revealed that *TbFlabarinL* is found not only within the soluble cytoplasmic and membrane fractions but also within the

cytoskeletal fractions both before and after separation of the flagella from the cytoskeleton (Fig. 3.16B)

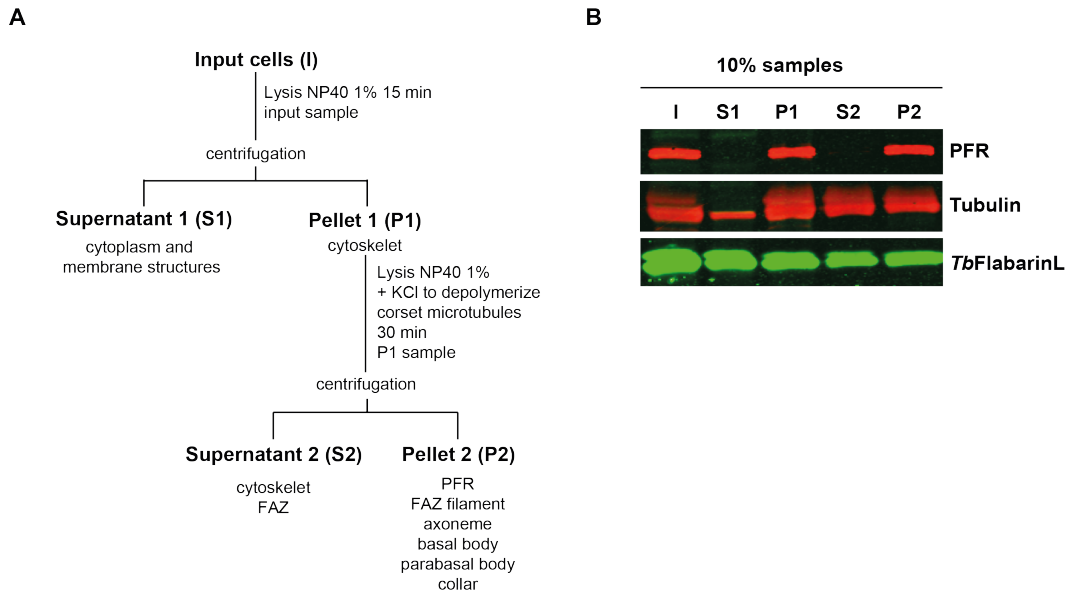


Figure 3.16. Biochemical cell fractionation of *TbFlabarinL*.

(A) Fractionation scheme: BSF cells were extracted in non-ionic detergent, after which an input sample (I) was taken. The cells were then separated by centrifugation into a detergent-soluble supernatant (S1) and detergent-insoluble cytoskeletal pellet (P1). The P1 fraction was solubilized in high salt to depolymerize corset microtubules, and further separated by centrifugation into S2 and P2 fractions. **(B)** Fractionation of *TbFlabarinL*. Equal fractions (10%) were loaded on a gel and analyzed by immunoblotting. Anti-PFR, TAT1 anti-tubulin and *TbFlabarinL* specific antibodies were used. *TbFlabarinL* was found in all fractions.

This result corroborates the observations described in previous experiments, which suggested a dual interaction with the flagellar membrane as well as with the structural components of the flagellum such as the PFR.

4 Discussion

Trypanosomes shuttle between vertebrate host and insect vector during their complex life cycle. In order to survive in such completely different environments, they possess very sophisticated adaptation machinery. Previously, we used a large scale proteomic approach to systematically understand the changes on the cellular level⁵³. Nevertheless, a detailed work on single components is necessary to provide information about adaptation mechanisms on the molecular level. Here we have performed a thorough characterization of a BSF stage specific putative flagellar host adaptation factor (Tb927.11.2400) that was identified in a SILAC-based comparative proteome study⁵³. It shares a 38% amino acid identity with *TbFlabarin* (Tb927.11.2410), a PCF stage specific⁵³ flagellar BAR domain protein. Tb927.11.2400 possesses no BAR domain *per se* and this is why we named it *TbFlabarin Like* (*TbFlabarinL*). Flabarin was for the first time described in *L. donovani* as a flagellar BAR domain protein⁶⁹. *LdFlabarin* is targeted to the flagellum by a potential N-terminal acylation site together with a central BAR domain for membrane association and the C-terminal domain needed for the flagellar specificity. It forms a helicoidal structure from the base to the tip of the flagellum⁶⁹. *In vitro* experiments suggest a morphogenetic and structural function since recombinant *LdFlabarin* associates with liposomes and triggers tubule formation⁶⁹. Recently, formation of membranous nanotubes was reported in *T. brucei*⁶⁰. Those nanotubes originate from the flagellar membrane and dissociate into free extracellular vesicles (EVs). The protein composition of isolated EVs was determined by mass spectrometry and revealed the presence of *TbFlabarinL* together with 155 other proteins⁶⁰. *TbFlabarinL* could be involved in the nanotubes/EVs formation or play a role in the fusion ability of the vesicles with other trypanosomes or erythrocytes or have an influence on the contents of the vesicles.

TbFlabarinL and *TbFlabarin* are both found adjacent on the chromosome 11. We assume that *TbFlabarinL* is the result of a gene duplication event that occurred in African trypanosomes. However, there are two exceptions: *T. congolense* and *T. equiperdum*. This could be explained by the unique life cycles of these two species. In contrast to *T. brucei*, *T. congolense* is a strictly intravascular parasite and does not traverse different tissues¹⁰³. *T. equiperdum* is essentially a tissue parasite in the reproductive system of *Equidae* family animals with a very low parasitemia in the blood and it is transmitted venereally¹⁰⁴. While the BSF stage upregulation suggested an

essential role of *TbFlabarinL* in the mammalian host, gene depletion and deletion experiments revealed that *TbFlabarinL* is not an essential gene for the growth and differentiation of trypanosomes in the cell culture. A pilot experiment in mice indicated that *TbFlabarinL* is dispensable during the first wave of parasitemia⁹⁹. Based on the distribution of *TbFlabarinL* across the different trypanosomatida species, we speculate that *TbFlabarinL* could be a part of adaptation to the lifestyle of African trypanosomes, in particular to their ability to leave the bloodstream in the mammalian host and migrate through different tissues in the advanced stages of the infection.

We generated a *TbFlabarinL* specific antibody and could detect *TbFlabarinL* in the flagellum in a discontinuous pattern. The flagellum is in direct contact with the environment and mediates interaction between the parasite and its host. Signaling molecules of the cAMP pathway such as BSF-specific adenylate cyclase ESAG4¹⁰⁵ or PCF specific adenylate cyclases (ACP1-5)⁶⁷ localize to the flagellar membrane. Masking the N-terminal end of *TbFlabarinL* with an epitope tag resulted in mislocalization of the protein. This provided an indirect evidence for the importance of the N-terminal sequence in tethering *TbFlabarinL* to the flagellar membrane. A closer inspection of the *TbFlabarinL* N-terminus allowed us to hypothesize that the presence of positively charged lysines and potentially myristoylated glycine and palmitoylated cysteine might be important for targeting *TbFlabarinL* to the flagellar membrane as shown previously for FCaBP in *T. cruzi*⁶⁶. Besides *TbFlabarinL*, other *T. brucei* flagellar membrane proteins such as arginine kinase 3 (AK3), *TbCaf17*, *TbCaf24* and *TbCaf44* share similar flagellar membrane address with the FCaBP⁶⁸. In addition, BAR domain associates *LdFlabarin* with the flagellar membrane⁶⁹. A structural model of both *TbFlabarinL* and *TbFlabarin* predicted a coiled coil helical architecture identical with *LdFlabarin* despite a missing BAR domain *per se* and suggested a membrane association. The discontinuous *TbFlabarinL* localization pattern could be explained by a potential association of the *TbFlabarinL* with the lipid rafts of the flagellar membrane due to the presence of dual acylation. Dually acylated proteins have been shown to prefer association with membrane microdomains enriched in sphingolipids and cholesterol (reviewed in¹⁰⁶). Co-immunoprecipitation using anti-*TbFlabarinL* specific antibody identified PAR1 as an interacting partner of *TbFlabarinL*. PAR1 is a component of the PFR and unlike *TbFlabarinL*, it was detected in a comparative proteomic study¹⁰² together with 20 novel components of the PFR. Cell fractionation revealed that *TbFlabarinL* is present not only in the

detergent soluble fraction but also it is tightly associated with the isolated flagella and cytoskeletal fractions containing PFR, which is in concordance with the predicted flagellar membrane localization as well as the result of the co-immunoprecipitation experiment. We suggest that the association of *TbFlabarinL* with the flagellar membrane might be only transient and function via a myristoyl switch mechanism, where the exposure of the myristate moiety could be ligand mediated as it is in the case of ADP ribosylation factor 1 (Arf1)¹⁰⁷. The binding of Arf1 to the membrane is regulated by guanine nucleotide (GDP). When GDP is bound, the myristoylated N-terminal helix is sheltered in a hydrophobic groove of Arf1 and dissociates from the membrane¹⁰⁸. Likewise when a ligand binds to *TbFlabarinL*, it might dissociate from the membrane and interact with the cytoskeletal components of the flagellum.

In this study we present a characterization of two flabarin orthologs in *T. brucei* with a major focus on *TbFlabarinL*, which is BSF stage specific in contrast to PCF specific *TbFlabarin*. We propose that African trypanosomes retained *TbFlabarinL* as an adaptation to the life in the mammalian host. Further research is still needed to fully understand the function of flabarins in trypanosomes.

5 References

1. Jensen, R. E. & Englund, P. T. Network news: the replication of kinetoplast DNA. *Annu. Rev. Microbiol.* **66**, 473–91 (2012).
2. H. Lopes, A. *et al.* Trypanosomatids: Odd Organisms, Devastating Diseases. *Open Parasitol. J.* **4**, (2010).
3. Kaye, P. & Scott, P. Leishmaniasis: complexity at the host-pathogen interface. *Nat. Rev. Microbiol.* **9**, 604–15 (2011).
4. World Health Organization: Leishmaniasis. <<http://www.who.int/mediacentre/factsheets/fs375/en/>>
5. World Health Organization: Chagas disease (American trypanosomiasis). [<http://www.who.int/mediacentre/factsheets/fs340/en/>]. at <<http://www.who.int/mediacentre/factsheets/fs340/en/>>
6. WHO | Trypanosomiasis, human African (sleeping sickness). at <<http://www.who.int/mediacentre/factsheets/fs259/en/>>
7. De Greef, C. & Hamers, R. The serum resistance-associated (SRA) gene of *Trypanosoma brucei rhodesiense* encodes a variant surface glycoprotein-like protein. *Mol. Biochem. Parasitol.* **68**, 277–284 (1994).
8. Rifkin, M. R. Identification of the trypanocidal factor in normal human serum: high density lipoprotein. *Proc. Natl. Acad. Sci. U. S. A.* **75**, 3450–4 (1978).
9. Pays, E. & Vanhollebeke, B. Human innate immunity against African trypanosomes. *Curr. Opin. Immunol.* **21**, 493–8 (2009).
10. Organization, W. H. & WHO Expert Committee on the Control and Surveillance of Human African Trypanosomiasis (2013: Geneva, S. Control and surveillance of human African trypanosomiasis: report of a WHO expert committee. (2013). at <<http://www.who.int/iris/handle/10665/95732>>
11. Franco, J. R., Simarro, P. P., Diarra, A. & Jannin, J. G. Epidemiology of human African trypanosomiasis. *Clin. Epidemiol.* **6**, 257–75 (2014).
12. Parsons, M. Glycosomes: parasites and the divergence of peroxisomal purpose. *Mol. Microbiol.* **53**, 717–24 (2004).

13. Benne, R. RNA editing in trypanosomes. *Eur. J. Biochem.* **221**, 9–23 (1994).
14. Ogbadoyi, E. O., Robinson, D. R. & Gull, K. A high-order transmembrane structural linkage is responsible for mitochondrial genome positioning and segregation by flagellar basal bodies in trypanosomes. *Mol. Biol. Cell* **14**, 1769–79 (2003).
15. Field, M. C. & Carrington, M. The trypanosome flagellar pocket. *Nat. Rev. Microbiol.* **7**, 775–86 (2009).
16. Overath, P. & Engstler, M. Endocytosis, membrane recycling and sorting of GPI-anchored proteins: *Trypanosoma brucei* as a model system. *Mol. Microbiol.* **53**, 735–44 (2004).
17. Namangala, B. How the African trypanosomes evade host immune killing. *Parasite Immunol.* **33**, 430–7 (2011).
18. Marcello, L. & Barry, J. D. Analysis of the VSG gene silent archive in *Trypanosoma brucei* reveals that mosaic gene expression is prominent in antigenic variation and is favored by archive substructure. *Genome Res.* **17**, 1344–52 (2007).
19. Hertz-Fowler, C. *et al.* Telomeric expression sites are highly conserved in *Trypanosoma brucei*. *PLoS One* **3**, e3527 (2008).
20. Horn, D. & McCulloch, R. Molecular mechanisms underlying the control of antigenic variation in African trypanosomes. *Curr. Opin. Microbiol.* **13**, 700–5 (2010).
21. Borst, P. & Rudenko, G. Antigenic variation in African trypanosomes. *Science (80-.)*. **264**, 1872–1873 (1994).
22. Borst, P. Control of VSG gene expression sites in *Trypanosoma brucei*. *Mol. Biochem. Parasitol.* **91**, 67–76 (1998).
23. Rudenko, G. Mechanisms Mediating Antigenic Variation in *Trypanosoma brucei*. *Mem. Inst. Oswaldo Cruz* **94**, 235–237 (1999).
24. Morrison, L. J., Marcello, L. & McCulloch, R. Antigenic variation in the African trypanosome: molecular mechanisms and phenotypic complexity. *Cell. Microbiol.* **11**, 1724–34 (2009).
25. Donelson, J. Multiple mechanisms of immune evasion by African trypanosomes. *Mol. Biochem. Parasitol.* **91**, 51–66 (1998).

26. Opperdoes, F. R. & Borst, P. Localization of nine glycolytic enzymes in a microbody-like organelle in *Trypanosoma brucei*: The glycosome. *FEBS Lett.* **80**, 360–364 (1977).
27. Bienen, E. J., Hammadi, E. & Hill, G. C. *Trypanosoma brucei*: Biochemical and morphological changes during in vitro transformation of bloodstream to procyclic-trypomastigotes. *Exp. Parasitol.* **51**, 408–417 (1981).
28. Vassella, E., Reuner, B., Yutzy, B. & Boshart, M. Differentiation of African trypanosomes is controlled by a density sensing mechanism which signals cell cycle arrest via the cAMP pathway. *J. Cell Sci.* **110** (Pt 2), 2661–71 (1997).
29. Vickerman, K. Polymorphism and Mitochondrial Activity In Sleeping Sickness Trypanosomes. *Nature* **208**, 762–766 (1965).
30. Roditi, I. *et al.* Procyclin gene expression and loss of the variant surface glycoprotein during differentiation of *Trypanosoma brucei*. *J. Cell Biol.* **108**, 737–46 (1989).
31. Hecker, H. Application of morphometry to pathogenic trypanosomes (protozoa, mastigophora). *Pathol. Res. Pract.* **166**, 203–17 (1980).
32. Tetley, L. & Vickerman, K. Differentiation in *Trypanosoma brucei*: host-parasite cell junctions and their persistence during acquisition of the variable antigen coat. *J. Cell Sci.* **74**, 1–19 (1985).
33. Vickerman, K. Developmental cycles and biology of pathogenic trypanosomes. *Br. Med. Bull.* **41**, 105–114 (1985).
34. Lukeš, J., Skalický, T., Týč, J., Votýpka, J. & Yurchenko, V. Evolution of parasitism in kinetoplastid flagellates. *Mol. Biochem. Parasitol.* **195**, 115–22 (2014).
35. Berriman, M. The Genome of the African Trypanosome *Trypanosoma brucei*. *Science* (80-.). **309**, 416–422 (2005).
36. Ivens, A. C. *et al.* The genome of the kinetoplastid parasite, *Leishmania major*. *Science* **309**, 436–42 (2005).
37. El-Sayed, N. M. *et al.* The genome sequence of *Trypanosoma cruzi*, etiologic agent of Chagas disease. *Science* **309**, 409–15 (2005).

38. Peacock, C. S. *et al.* Comparative genomic analysis of three Leishmania species that cause diverse human disease. *Nat. Genet.* **39**, 839–47 (2007).
39. Barry, S., Towers, K. & Vaughan, S. Screening ciliopathy genes in the model organism Trypanosoma brucei. *Cilia* **1**, P81 (2012).
40. Li, Z. Regulation of the cell division cycle in Trypanosoma brucei. *Eukaryot. Cell* **11**, 1180–90 (2012).
41. Ngo, H., Tschudi, C., Gull, K. & Ullu, E. Double-stranded RNA induces mRNA degradation in Trypanosoma brucei. *Proc. Natl. Acad. Sci.* **95**, 14687–14692 (1998).
42. Fire, A. *et al.* Potent and specific genetic interference by double-stranded RNA in Caenorhabditis elegans. *Nature* **391**, 806–11 (1998).
43. Kelly, S. *et al.* Functional genomics in Trypanosoma brucei: A collection of vectors for the expression of tagged proteins from endogenous and ectopic gene loci. *Mol. Biochem. Parasitol.* **154**, 103–109 (2007).
44. Wirtz, E., Leal, S., Ochatt, C. & Cross, G. M. A tightly regulated inducible expression system for conditional gene knock-outs and dominant-negative genetics in Trypanosoma brucei. *Mol. Biochem. Parasitol.* **99**, 89–101 (1999).
45. Akiyoshi, B. & Gull, K. Evolutionary cell biology of chromosome segregation: insights from trypanosomes. *Open Biol.* **3**, 130023 (2013).
46. Siegel, T. N., Hekstra, D. R., Wang, X., Dewell, S. & Cross, G. A. M. Genome-wide analysis of mRNA abundance in two life-cycle stages of Trypanosoma brucei and identification of splicing and polyadenylation sites. *Nucleic Acids Res.* **38**, 4946–57 (2010).
47. Queiroz, R., Benz, C., Fellenberg, K., Hoheisel, J. D. & Clayton, C. Transcriptome analysis of differentiating trypanosomes reveals the existence of multiple post-transcriptional regulons. *BMC Genomics* **10**, 495 (2009).
48. Kabani, S. *et al.* Genome-wide expression profiling of in vivo-derived bloodstream parasite stages and dynamic analysis of mRNA alterations during synchronous differentiation in Trypanosoma brucei. *BMC Genomics* **10**, 427 (2009).
49. Clayton, C. The regulation of trypanosome gene expression by RNA-binding proteins. *PLoS Pathog.* **9**, e1003680 (2013).

50. Manful, T., Fadda, A. & Clayton, C. The role of the 5'-3' exoribonuclease XRNA in transcriptome-wide mRNA degradation. *RNA* **17**, 2039–47 (2011).
51. Vasquez, J.-J., Hon, C.-C., Vanselow, J. T., Schlosser, A. & Siegel, T. N. Comparative ribosome profiling reveals extensive translational complexity in different *Trypanosoma brucei* life cycle stages. *Nucleic Acids Res.* **42**, 3623–37 (2014).
52. Jensen, B. C. *et al.* Extensive stage-regulation of translation revealed by ribosome profiling of *Trypanosoma brucei*. *BMC Genomics* **15**, 911 (2014).
53. Butter, F. *et al.* Comparative proteomics of two life cycle stages of stable isotope-labeled *Trypanosoma brucei* reveals novel components of the parasite's host adaptation machinery. *Molecular & Cellular Proteomics* (2012).
54. Ralston, K. S., Kabututu, Z. P., Melehani, J. H., Oberholzer, M. & Hill, K. L. The *Trypanosoma brucei* flagellum: moving parasites in new directions. *Annu. Rev. Microbiol.* **63**, 335–62 (2009).
55. Langousis, G. & Hill, K. L. Motility and more: the flagellum of *Trypanosoma brucei*. *Nat. Rev. Microbiol.* **12**, 505–18 (2014).
56. Subota, I. *et al.* Proteomic analysis of intact flagella of procyclic *Trypanosoma brucei* cells identifies novel flagellar proteins with unique sub-localization and dynamics. *Mol. Cell. Proteomics* **13**, 1769–86 (2014).
57. Oberholzer, M. *et al.* Independent analysis of the flagellum surface and matrix proteomes provides insight into flagellum signaling in mammalian-infectious *Trypanosoma brucei*. *Mol. Cell. Proteomics* **10**, M111.010538 (2011).
58. Shimogawa, M. M. *et al.* Cell surface proteomics provides insight into stage-specific remodeling of the host-parasite interface in *Trypanosoma brucei*. *Mol. Cell. Proteomics* M114.045146– (2015). doi:10.1074/mcp.M114.045146
59. Tetley, L. & Vickerman, K. Differentiation in *Trypanosoma brucei*: host-parasite cell junctions and their persistence during acquisition of the variable antigen coat. *J. Cell Sci.* **74**, 1–19 (1985).

60. Szempruch, A. J. *et al.* Extracellular Vesicles from *Trypanosoma brucei* Mediate Virulence Factor Transfer and Cause Host Anemia. *Cell* **164**, 246–257 (2016).
61. Emmer, B. T., Daniels, M. D., Taylor, J. M., Epting, C. L. & Engman, D. M. Calflagin inhibition prolongs host survival and suppresses parasitemia in *Trypanosoma brucei* infection. *Eukaryot. Cell* **9**, 934–42 (2010).
62. Proto, W. R. *et al.* *Trypanosoma brucei* metacaspase 4 is a pseudopeptidase and a virulence factor. *J. Biol. Chem.* **286**, 39914–25 (2011).
63. Salmon, D. *et al.* Adenylate cyclases of *Trypanosoma brucei* inhibit the innate immune response of the host. *Science* **337**, 463–6 (2012).
64. Webb, H. The GPI-Phospholipase C of *Trypanosoma brucei* Is Nonessential But Influences Parasitemia in Mice. *J. Cell Biol.* **139**, 103–114 (1997).
65. Serricchio, M. *et al.* Flagellar membranes are rich in raft-forming phospholipids. *Biol. Open* (2015). doi:10.1242/bio.011957
66. Maric, D. *et al.* Molecular determinants of ciliary membrane localization of *Trypanosoma cruzi* flagellar calcium-binding protein. *J. Biol. Chem.* **286**, 33109–17 (2011).
67. Saada, E. A. *et al.* Insect stage-specific receptor adenylate cyclases are localized to distinct subdomains of the *Trypanosoma brucei* Flagellar membrane. *Eukaryot. Cell* **13**, 1064–76 (2014).
68. Ooi, C.-P. *et al.* The Flagellar Arginine Kinase in *Trypanosoma brucei* Is Important for Infection in Tsetse Flies. *PLoS One* **10**, e0133676 (2015).
69. Lefebvre, M. *et al.* LdFlabarin, a new BAR domain membrane protein of *Leishmania flagellum*. *PLoS One* **8**, e76380 (2013).
70. Aslett, M. *et al.* TriTrypDB: a functional genomic resource for the Trypanosomatidae. *Nucleic Acids Res.* **38**, D457–62 (2010).
71. Papadopoulos, J. S. & Agarwala, R. COBALT: constraint-based alignment tool for multiple protein sequences. *Bioinformatics* **23**, 1073–9 (2007).
72. Robert, X. & Gouet, P. Deciphering key features in protein structures with the new ENDscript server. *Nucleic Acids Res.* **42**, W320–4 (2014).

73. Kelley, L. A., Mezulis, S., Yates, C. M., Wass, M. N. & Sternberg, M. J. E. The Phyre2 web portal for protein modeling, prediction and analysis. *Nat. Protoc.* **10**, 845–858 (2015).
74. Pettersen, E. F. *et al.* UCSF Chimera--a visualization system for exploratory research and analysis. *J. Comput. Chem.* **25**, 1605–12 (2004).
75. Kohl, L., Sherwin, T. & Gull, K. Assembly of the paraflagellar rod and the flagellum attachment zone complex during the *Trypanosoma brucei* cell cycle. *J. Eukaryot. Microbiol.* **46**, 105–9
76. Woods, A. *et al.* Definition of individual components within the cytoskeleton of *Trypanosoma brucei* by a library of monoclonal antibodies. *J. Cell Sci.* **93**, 491–500 (1989).
77. Bastin, P., Bagherzadeh, A., Matthews, K. R. & Gull, K. A novel epitope tag system to study protein targeting and organelle biogenesis in *Trypanosoma brucei*. *Mol. Biochem. Parasitol.* **77**, 235–239 (1996).
78. Morriswood, B. *et al.* Novel bilobe components in *Trypanosoma brucei* identified using proximity-dependent biotinylation. *Eukaryot. Cell* **12**, 356–67 (2013).
79. Alibu, V. P., Storm, L., Haile, S., Clayton, C. & Horn, D. A doubly inducible system for RNA interference and rapid RNAi plasmid construction in *Trypanosoma brucei*. *Mol. Biochem. Parasitol.* **139**, 75–82 (2005).
80. Alsford, S., Kawahara, T., Glover, L. & Horn, D. Tagging a *T. brucei* RRNA locus improves stable transfection efficiency and circumvents inducible expression position effects. *Mol. Biochem. Parasitol.* **144**, 142–8 (2005).
81. Hirumi, H. & Hirumi, K. Continuous cultivation of *Trypanosoma brucei* blood stream forms in a medium containing a low concentration of serum protein without feeder cell layers. *J. Parasitol.* **75**, 985–9 (1989).
82. Vassella, E. & Boshart, M. High molecular mass agarose matrix supports growth of bloodstream forms of pleomorphic *Trypanosoma brucei* strains in axenic culture. *Mol. Biochem. Parasitol.* **82**, 91–105 (1996).

83. Brun, R. & Schönenberger. Cultivation and in vitro cloning or procyclic culture forms of *Trypanosoma brucei* in a semi-defined medium. Short communication. *Acta Trop.* **36**, 289–92 (1979).
84. Schumann Burkard, G., Jutzi, P. & Roditi, I. Genome-wide RNAi screens in bloodstream form trypanosomes identify drug transporters. *Mol. Biochem. Parasitol.* **175**, 91–4 (2011).
85. Vassella, E. *et al.* Deletion of a novel protein kinase with PX and FYVE-related domains increases the rate of differentiation of *Trypanosoma brucei*. *Mol. Microbiol.* **41**, 33–46 (2001).
86. MacGregor, P., Rojas, F., Dean, S. & Matthews, K. R. Stable transformation of pleomorphic bloodstream form *Trypanosoma brucei*. *Mol. Biochem. Parasitol.* **190**, 60–2 (2013).
87. Overath, P., Czichos, J. & Haas, C. The effect of citrate/ cis-aconitate on oxidative metabolism during transformation of *Trypanosoma brucei*. *Eur. J. Biochem.* **160**, 175–182 (1986).
88. Alsford, S. & Horn, D. Single-locus targeting constructs for reliable regulated RNAi and transgene expression in *Trypanosoma brucei*. *Mol. Biochem. Parasitol.* **161**, 76–9 (2008).
89. Shevchenko, A., Tomas, H., Havlis, J., Olsen, J. V & Mann, M. In-gel digestion for mass spectrometric characterization of proteins and proteomes. *Nat. Protoc.* **1**, 2856–60 (2006).
90. Cox, J. & Mann, M. MaxQuant enables high peptide identification rates, individualized p.p.b.-range mass accuracies and proteome-wide protein quantification. *Nat. Biotechnol.* **26**, 1367–72 (2008).
91. Esson, H. J. *et al.* Morphology of the trypanosome bilobe, a novel cytoskeletal structure. *Eukaryot. Cell* **11**, 761–72 (2012).
92. Morriswood, B. & Schmidt, K. A MORN-repeat protein facilitates protein entry into the flagellar pocket of *Trypanosoma brucei*. *Eukaryot. Cell* EC.00094–15– (2015). doi:10.1128/EC.00094-15
93. Mim, C. & Unger, V. M. Membrane curvature and its generation by BAR proteins. *Trends Biochem. Sci.* **37**, 526–33 (2012).
94. Siegel, T. N. *et al.* Four histone variants mark the boundaries of polycistronic transcription units in *Trypanosoma brucei*. *Genes Dev.* **23**, 1063–76 (2009).

95. Li, L., Stoeckert, C. J. & Roos, D. S. OrthoMCL: identification of ortholog groups for eukaryotic genomes. *Genome Res.* **13**, 2178–89 (2003).
96. Chen, F., Mackey, A. J., Stoeckert, C. J. & Roos, D. S. OrthoMCL-DB: querying a comprehensive multi-species collection of ortholog groups. *Nucleic Acids Res.* **34**, D363–8 (2006).
97. Dejung, M. *et al.* Quantitative Proteomics Uncovers Novel Factors Involved in Developmental Differentiation of *Trypanosoma brucei*. *PLoS Pathog.* **12**, e1005439 (2016).
98. Alsford, S. & Horn, D. Single-locus targeting constructs for reliable regulated RNAi and transgene expression in *Trypanosoma brucei*. *Mol. Biochem. Parasitol.* **161**, 76–9 (2008).
99. Nicole Eisenhuth. Characterization of novel components of *Trypanosoma brucei*'s host adaptation machinery. (Julius Maximilian University Wuerzburg, 2015).
100. Saborio, J. L. *et al.* Isolation and characterization of paraflagellar proteins from *Trypanosoma cruzi*. *J. Biol. Chem.* **264**, 4071–4075 (1989).
101. Fouts, D. L. *et al.* Evidence for Four Distinct Major Protein Components in the Paraflagellar Rod of *Trypanosoma cruzi*. *J. Biol. Chem.* **273**, 21846–21855 (1998).
102. Portman, N., Lacomble, S., Thomas, B., McKean, P. G. & Gull, K. Combining RNA interference mutants and comparative proteomics to identify protein components and dependences in a eukaryotic flagellum. *J. Biol. Chem.* **284**, 5610–9 (2009).
103. Banks, K. L. Binding of *Trypanosoma congolense* to the Walls of Small Blood Vessels*. *J. Protozool.* **25**, 241–245 (1978).
104. Claes, F., Büscher, P., Touratier, L. & Goddeeris, B. M. *Trypanosoma equiperdum*: master of disguise or historical mistake? *Trends Parasitol.* **21**, 316–21 (2005).
105. Paindavoine, P. *et al.* A gene from the variant surface glycoprotein expression site encodes one of several transmembrane adenylate cyclases located on the flagellum of *Trypanosoma brucei*. *Mol. Cell. Biol.* **12**, 1218–25 (1992).

106. Resh, M. D. Fatty acylation of proteins: new insights into membrane targeting of myristoylated and palmitoylated proteins. *Biochim. Biophys. Acta - Mol. Cell Res.* **1451**, 1–16 (1999).
107. Boman, A. & Kahn, R. Arf proteins: the membrane traffic police? *Trends Biochem. Sci.* **20**, 147–150 (1995).
108. Amor, J. C., Harrison, D. H., Kahn, R. A. & Ringe, D. Structure of the human ADP-ribosylation factor 1 complexed with GDP. *Nature* **372**, 704–8 (1994).